creative commons
COMMONS DEED

저작자표시-비영리-변경금지 2.0 대한민국

이용자는 아래의 조건을 따르는 경우에 한하여 자유롭게

- 이 저작물을 복제, 배포, 전송, 전시, 공연 및 방송할 수 있습니다.

다음과 같은 조건을 따라야 합니다:

**저작자표시**. 귀하는 원저작자를 표시하여야 합니다.

**비영리**. 귀하는 이 저작물을 영리 목적으로 이용할 수 없습니다.

**변경금지**. 귀하는 이 저작물을 개작, 변형 또는 가공할 수 없습니다.

- 귀하는, 이 저작물의 재이용이나 배포의 경우, 이 저작물에 적용된 이용허락조건을 명확하게 나타내어야 합니다.
- 저작권자로부터 별도의 허가를 받으면 이러한 조건들은 적용되지 않습니다.

**저작권법에 따른 이용자의 권리는 위의 내용에 의하여 영향을 받지 않습니다.**

이것은 이용허락규약(Legal Code)을 이해하기 쉽게 요약한 것입니다.

Disclaimer

dCollection

공학박사학위논문

# 전해 디포지션을 이용한 금속의 초소수성 표면 제작

**Fabrication of a Super-hydrophobic Surface on Metal Using Electrodeposition**

**2014년 2월**


**서울대학교 대학원**

**기계항공공학부**

**권 민 호**

# FABRICATION OF A SUPER-HYDROPHOBIC SURFACE ON METAL USING ELECTRODEPOSITION

DISSERTATION

SUBMITTED TO THE SCHOOL OF MECHANICAL

AND AEROSPACE ENGINEEERING AND THE COMMITTEE ON

GRADUATE STUDIES OF SEOUL NATIONAL UNIVERSITY

IN PARTIAL FULFILLMENT OF THE REQUIREMENTS

FOR THE DEGREE OF DOCTOR OF PHILOSOPHY

Min Ho Kwon

October 2013

# 전해 디포지션을 이용한
# 금속의 초소수성 표면 제작

**Fabrication of a Super-hydrophobic Surface on Metal Using Electrodeposition**

**지도교수 주 종 남**

**이 논문을 공학박사 학위논문으로 제출함**

**2013년 10월**


**서울대학교 대학원**

**기계항공공학부**

**권 민 호**


**권민호의 공학박사 학위논문을 인준함**

**2013년 12월**

**위 원 장 : _____**

**부위원장 : _____**

**위 원 : _____**

**위 원 : _____**

**위 원 : _____**

*To my parents and my family*

# Abstract

Min Ho Kwon

School of Mechanical and Aerospace Engineering

The Graduate School

Seoul National University

In this research, the fabrication process of a super-hydrophobic metallic surface using electrodeposition was investigated. The super-hydrophobic metallic surfaces are expected to broaden the practical application field of super-hydrophobicity that has been limited to some types of films for self-cleaning and preventing the pollution. Re-entrant structure and hierarchical structure have advantages in water repellent property of surfaces. Fabrication processes using electrodeposition that has an advantage in diversifying the surface morphology and property were

proposed. The re-entrant structure plays an important role in forming a super-hydrophobic surface on intrinsically hydrophilic material. A micro pillar array with a re-entrant structure was fabricated through a sequential process of laser ablation, insulating, mechanical polishing and electrodeposition. Spacing of the micro pillars in the array played a major role in hydrophobicity of the structure that was confirmed by measuring the water contact angle. Surface morphology changed relative to the parameters of the laser ablation process and electrodeposition process. Under gradual increase in current density during the electrodeposition process, surface morphology roughness was maximized for fabricating a super-hydrophobic surface. Material combinations of substrate and deposited material were also investigated. Fabrication process for hierarchical structure is consisted of laser ablation for micro-structuring and electrodeposition for hierarchical structuring. Under excessive current density condition in electrodeposition, hierarchical structure was fabricated with low surface energy resulting from copper oxide. Fabricated structures with more than a hundred micrometer in depth have a super-hydrophobicity. The role of copper oxide and

hierarchical structure were confirmed by oxidation test of fabricated structures because copper oxide had an undetectable thickness by XRD and XPS. To evaluate the dynamic robustness of hydrophobicity, experiments with dynamic contact angle and squeezing test were carried out.

Keywords: Super-hydrophobicity, Wettability, Metal, Electrodeposition, Re-entrant structure, Hierarchical structure

Student number: 2009-30159

# Contents

**Abstract……i**

**Contents……iv**

**List of Figures……...….vi**

**List of Tables……...x**

**1. Introduction……1**

1.1 Research background

1.2 Research purpose and dissertation overview

**2. Super-hydrophobicity……9**

2.1 Principle

2.2 Hierarchical structure

2.3 Re-entrant structure

**3. Electrodeposition……..18**

3.1 Fundamental concepts

3.2 Deposition of copper

3.3 Morphology

**4. Fabrication process for re-entrant structure……26**

4.1 Experimental setup

4.2 Fabrication process

4.3 Water contact angle relative to the spacing of the micro pillar array

4.4 Water contact angle relative to current density in electrodeposition

4.5 Material combinations of substrate and deposited material

**5. Fabrication process for hierarchical structure……..…55**

5.1 Fabrication process

5.2 Effect of copper oxide

5.3 Effect of hierarchical structure

5.4 Water contact angle relative to the depth of micro structure

**6. Dynamic robustness of hydrophobicity……..75**

6.1 Sliding test

6.2 Squeezing test

**7. Conclusion…….90**

**References…….93**

**국문 초록……..99**

# List of Figures

**Figure 2.1** Schematic of a liquid drop showing the quantities in Young's equation

**Figure 2.2** Schematic of the wetting in the Cassie-Baxter model

**Figure 2.3** Schematic of the wetting in the Wenzel model

**Figure 2.4** Schematic diagrams of liquid-vapor inter face on different structures

**Figure 3.1** Schematic of electrodeposition of copper on substrate in a copper sulfate bath

**Figure 3.2** SEM images of electrodes deposited by the local electrochemical deposition process

**Figure 4.1** Schematic of experimental setup for laser ablation and electrodeposition

**Figure 4.2** Schematic of the sequential fabrication process

**Figure 4.3** Micro pillar array fabricated by laser ablation in 280 μm spacing ; (a) scanning path (b) SEM image at 45˚ tilt angle

**Figure 4.4** SEM image of the re-entrant structure array after electrodeposition at 45˚ tilt angle; laser ablation created 280 μm spacing of pillars and electrodeposition was accomplished at a current density of 640 $\mu A/mm^2$

**Figure 4.5** CCD image of water droplets on the re-entrant structure array and flat surface; laser ablation created 280 μm spacing of pillars and electrodeposition was accomplished at a current density of 640 $\mu A/mm^2$

**Figure 4.6** Schematic of liquid droplet on different local texture angle (a) local texture angle $\psi <$ water contact angle $\theta$ and (b) local texture angle $\psi >$ water contact angle $\theta$

**Figure 4.7** SEM image of fabricated re-entrant structure (side view)

**Figure 4.8** SEM image and water contact angle of micro pillar arrays fabricated using electrodeposition at the noted current densities (320 $\mu A/mm^2$ for 1 hour, 640 $\mu A/mm^2$ for 30 min, 1280 $\mu A/mm^2$ for 15 min) and spacing (180 μm, 280 μm, 380 μm); error range of water contact angles was $\pm 1^{\circ}$.

**Figure 4.9** Comparison between theoretical values (Cassie model and Wenzel model) and experimental values

**Figure 4.10** SEM image of surface fabricated by electrodeposition relative to current density (a) 320 $\mu A/mm^2$, (b) 640 $\mu A/mm^2$ and (c) 1280 $\mu A/mm^2$

**Figure 4.11** SEM image and water contact angle of micro pillar array fabricated using electrodeposition with a gradual increase in current density; experimental conditions are noted in Table 4.1

**Figure 4.12** SEM image and water contact angle of re-entrant structure array fabricated using sequential process including laser ablation, insulation, mechanical polishing and electrodeposition; (a) nickel deposition on stainless

steel and (b) copper deposition on copper

**Figure 5.1** SEM image and water contact angle of surface fabricated by electrodeposition relative to current density (a) 320 μA/mm$^2$, (b) 640 μA/mm$^2$ , (c) 1280 μA/mm$^2$ and (d) 2560 μA/mm$^2$

**Figure 5.2** Fabrication process for hierarchical structure

**Figure 5.3** SEM image and water contact angle of fabricated surface using fabrication process for hierarchical structure

**Figure 5.4** XRD patterns of deposited copper surface: (a) current density: 640 μA/mm$^2$ and (b) 2560 μA/mm$^2$

**Figure 5.5** Heat oxidized copper surfaces for 20 min; (No treatment, 100℃, 200℃, 300℃, 400℃, 500℃)

**Figure 5.6** Fabricated surface using sequential process of laser ablation, mechanical polishing and heat oxidation at 200℃

**Figure 5.7** Fabricated surface using sequential process of laser ablation, electrodeposition and heat oxidation at 200℃

**Figure 5.8** Hierarchical structure according to copper oxide removal

**Figure 5.9** SEM image and water contact angle of surface fabricated by fabrication process for hierarchical structure relative to average depth of micro structure (a) 10, (b) 30, (c) 65, (d) 135, (e) 200 and (f) 275 μm

**Figure 5.10** Surface profile of surface fabricated by fabrication process for hierarchical structure: average depth (a) 65 and (b) 135 μm

**Figure 5.11** SEM image and water contact angle of micro pillar arrays fabricated by fabrication process for hierarchical structure relative to spacing and average depth

**Figure 6.1** The captured images of advancing and receding angle by the dynamic sessile drop method: fabricated structure using hierarchical structure in (a) 180 μm, (b) 280 μm and (c) 380 μm spacing, and (d) re-entrant structure

**Figure 6.2** SEM image of tested structure and captured images of the sliding test: fabricated structure using hierarchical structure in (a) 180 μm, (b) 280 μm and (c) 380 μm spacing, and (d) re-entrant structure

**Figure 6.3** SEM image of tested structure and captured images of the squeezing test: fabricated structure using hierarchical structure in (a) 180 μm, (b) 280 μm and (c) 380 μm spacing, and (d) re-entrant structure

**Figure 6.4** Captured images of the squeezing test: fabricated surfaces with hierarchical structure in 180 μm spacing with (a) 700 μm gap and (b) 600 μm gap

**Figure** 6.5 Side views of the transition from Cassie to Wenzel state due to depinning and sag mechanisms in a pillar-type roughness geometry [30]

# List of Tables

**Table 4.1** Experimental conditions of electrodeposition with a gradual increase in current density; fractional numbers in parenthesis refer to the proportion of deposition in each step of the overall process.

**Table 6.1** Roll off angle and contact angle hysteresis of fabricated structure shown in Figure 6.1.

**Table 6.2** De-pinning and Sag transition criteria of fabricated structure using hierarchical structure

# Chapter 1

# Introduction

## 1.1 Research background

Recently, super-hydrophobic surfaces have been investigated by numerous researchers because of potential applications in self-cleaning, fog-resistance, drag reduction in microfluidics and prevention of corrosion [1]. Two types of fabrication methods for creating super-hydrophobic surfaces have been developed. In the case of hydrophobic material, high surface roughness can amplify the

hydrophobicity of the surface. In the case of hydrophilic material, surface coating that lowers surface energy is needed because roughening the surface makes it more hydrophilic. However, a surface coating of chemical material creates an aging effect. Aging in air leads to a hydrophobic surface, which differs from an untreated surface, both in surface composition and in wetting behavior [2]. Therefore, a durable super-hydrophobic surface should be made up of several physical structures and exclude chemical treatment. Re-entrant structure, such as a micro-hoodoo, mushroom-like topography is well known for its liquid repellent property. In this structure, net traction force of a liquid droplet is upward because of its re-entrant angle between the top surface and side wall of the structure. It has been used in super-oleophobicity due to the low surface tension of oil compared to water [3, 4]. Therefore, several studies have been conducted on the super-hydrophobicity on hydrophilic surfaces [5, 6]. However, these studies have been at a disadvantage of using a fabrication process that consists of a wafer-based process, which restricts the working environment.

Many attempts have been made to achieve a robust super-hydrophobic surface on metal [7-10]. A physical structure of micro- and nano-sized rough morphology was fabricated using micro-fabrication techniques, such as laser ablation, anodizing, sandblasting and electrochemical etching. Subsequently, the surface energy of the roughened surface was reduced through chemical treatment. Nonetheless, these methods are still subjected to aging problems resulting from the applied chemical treatment.

There have been studies on the fabrication of super-hydrophobic surface using electrodeposition. Sarkar et al. demonstrated that super-hydrophobic silver films on copper substrates can be created in just a one-steop process via galvanic reactions by immersing the substrates in silver nitrate solution containing benzoic acid [11]. Wang et al. present a fabrication method for constructing an environmentally stable super-hydrophobic metal fatty acid carboxylates surface coated with $Cu(CH_3(CH_2)_{12}COO)_2$ [12]. However, previous fabrication methods using electrodeposition included an organic compound.

In order to overcome the drawbacks and enhance the robustness of a super-hydrophobic surface, Bae et al. present a direct, one-step method for fabricating a dual-scale super-hydrophobic metallic surface using wire electrical discharge machining [13]. A micro scale sinusoidal pattern with a wavelength in hundredths of a micrometer and secondary roughness in the form of microcraters was fabricated using wire electrical discharge machining. However, the material used was Al 7075 alloy (duralumin), intrinsically hydrophobic. For these reasons, this fabrication method cannot be used with other metals that are intrinsically hydrophilic.

In this research, a micro-fabrication process using electrodeposition is introduced to obtain a hydrophobic metallic structure. The fabrication process can be performed in a general working environment, in contrast to other fabrication methods for a re-entrant structure such as MEMS technologies. In addition, a fabricated metallic structure has greater durability against heat and time lapse compared to a polymer-based structure and a chemical treatment to lower the

surface energy. The super-hydrophobic metallic surfaces are expected to broaden the practical application field of super-hydrophobicity that has been limited to some types of films for self-cleaning and preventing the pollution. The super-hydrophobic metallic structure without surface treatments can be applied to many industrial fields by its electrical and thermal properties.

## 1.2 Research purpose and dissertation overview

The purpose of this research is the development of the micro-fabrication process of super-hydrophobic metallic surfaces using electrodeposition. To achieve this goal, the sequential fabrication processes for re-entrant structure and hierarchical structure including laser ablation and electrodeposition were newly developed. The micro pillar arrays with re-entrant structures and hierarchical structures were fabricated at different micro pillar spacing and surface morphology of the deposited material. Further, the hydrophobicity of the fabricated surface was evaluated with respect to the water contact angle of deionized water droplets. To evaluate the hydrophobic robustness of fabricated structure, sliding test and squeezing test were investigated experimentally.

In chapter 2, super-hydrophobicity is presented. The basic principle of super-hydrophobicity and the representative physical structure for super-hydrophobicity such as hierarchical structure and re-entrant structure are presented.

In chapter 3, principles of electrodeposition are presented. Fundamental concepts, deposition of copper and surface morphology are presented.

In chapter 4, fabrication process for re-entrant structure is described. Experimental setup and fabrication process are explained in this chapter. Water contact angle relative to the spacing of the micro pillar array and current density are also presented.

In chapter 5, fabrication process for hierarchical structure is described. Experimental setup and fabrication process are explained in this chapter. Water contact angle relative to the spacing of the micro pillar array and current density are also presented.

In chapter 6, Dynamic robustness of hydrophobicity is analyzed. To evaluate the robustness, sliding test and squeezing test are presented.

In chapter 7, conclusion and discussion in this research are presented.

# Chapter 2

# Super-hydrophobicity

## 2.1 Principle

Super-hydrophobic surfaces, such as the leaves of the lotus plant, are those that are extremely difficult to wet. The contact angle of a water droplet exceeds 150 °. The contact angle is the angle, conventionally measured through the liquid, where a liquid/vapor interface meets a solid surface. A given system of solid, liquid, and vapor has a unique equilibrium contact angle. It quantifies the wettability of a

solid surface by a liquid via the Young's equation. Fig. 2.1 shows the schematic of a liquid drop and Young's equation.

On textured surface, there are two kinds of wetting state, leading to different apparent contact angles. First, liquid droplets can be partially supported by air between solid asperities much smaller than the size of droplets as shown in Fig. 2.2. In this case, an apparent contact angle is given by the Cassie-Baxter equation. On the other hand, there is another wetting regime in which the space between textured solid structures underneath droplets is fully wetted with liquids as shown in Fig. 2.3. The apparent contact angle in the fully-wetted is given by the Wenzel equation. The simple Cassie and Wenzel models provide a useful framework to understand high contact angles.

**Young's Equation:** $\boldsymbol{\gamma_{SV} = \gamma_{SL} + \gamma_{LV}\cos\theta}$

$\gamma_{SV}$: Solid-vapor interfacial energy

$\gamma_{SL}$: Solid-liquid interfacial energy

$\gamma_{LV}$: Liquid-vapor interfacial energy

θ: Contact angle determined by Young's Equation

**Figure 2.1** Schematic of a liquid drop showing the quantities in Young's equation

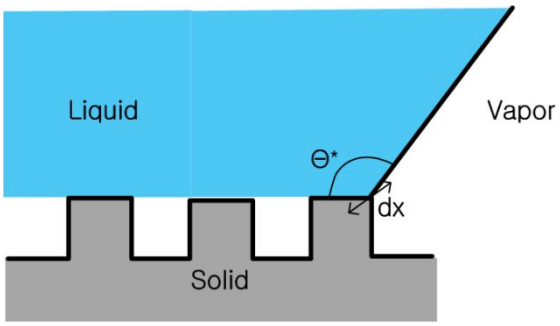


$$dF = f_1(\gamma_{SL} - \gamma_{SV})_1 dx + f_2(\gamma_{SL} - \gamma_{SV})_2 dx + \gamma_{LV}\cos\theta^* = 0$$

$$\boldsymbol{\cos\theta^* = f_1\cos\theta_1 + f_2\cos\theta_2}$$

$f_1$, $f_2$: Fractional surface areas

$\gamma_{SL}$: Solid-liquid surface tension

$\gamma_{LV}$: Liquid-vapor surface tension

$\gamma_{SV}$: Solid-vapor surface tension

$\theta$: Contact angle of flat surface

$\theta^*$: Contact angle of structured surface

**Figure 2.2** Schematic of the wetting in the Cassie-Baxter model

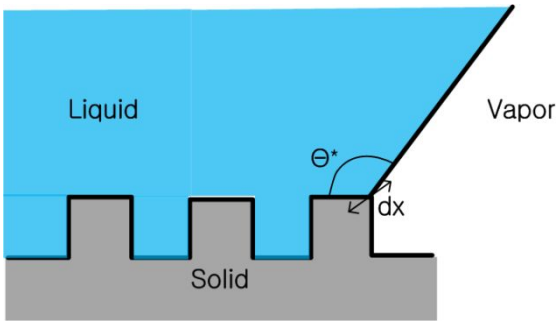


$$dF = r(\gamma_{SL} - \gamma_{SV})dx + \gamma_{LV}\cos\theta^* = 0$$

$$\boldsymbol{\cos\theta^* = r\,\frac{\gamma_{SV} - \gamma_{SL}}{\gamma_{LV}} = r\cos\theta}$$

$$r\ (\text{surface roughness factor}) = \frac{real\ surface\ area}{projected\ surface\ area} > 1$$

$\gamma_{SL}$: Solid-liquid surface tension

$\gamma_{LV}$: Liquid-vapor surface tension

$\gamma_{SV}$: Solid-vapor surface tension

$\theta$: Contact angle of flat surface

$\theta^*$: Contact angle of structured surface

**Figure 2.3** Schematic of the wetting in the Wenzel model

## 2.2 Hierarchical structure

The micro-nano hierarchical structure is well known for its advantages in fabricating a super-hydrophobic surface. Super-hydrophobic surfaces should be capable of forming a composite solid-liquid-air interface to achieve a large water contact angle. A hierarchical structure makes it possible for a greater composite interface that results in decreased contact area between the liquid droplet and the solid. In addition, the hierarchical structure can prevent the transformation of the composite interface into homogeneous interface from external factors such as perturbation and the scale of droplets [14]. Therefore, the techniques to make super-hydrophobic surfaces can be simply divided into two categories: making a rough surface from a low surface energy material and modifying a rough surface with a material of low surface energy [15].

## 2.3 Re-entrant structure

The re-entrant structure is especially indispensable for its water repellent property with intrinsically hydrophilic material. Therefore, effective manufacturing of a re-entrant structure is the main goal of the fabrication process. Figure 2.4 shows the re-entrant structure and its principle of water repellency [3, 4]. Figure 2.4 (a) and 2.4 (b) show the schematics of wetting on different physical structures that have the same chemical property. The re-entrant structure is a surface with concave topographic features where the local texture angle $\psi$ is smaller than 90˚, as shown in Figure 2.4 (b). If the contact angle $\theta$ of a hypothetical liquid is smaller than local texture angle $\psi$, the structure is considered to be fully wetted because the net traction force on the liquid-vapor interface is directed downward, as shown in Figure 2.4 (a). In the case of a re-entrant structure, shown in Figure 2.4 (b), the

structure plays a role in supporting the formation of a composite interface because the net traction force is directed upward. Many researchers have investigated similar kinds of surface structures for the large apparent contact angles [5, 6, 16].

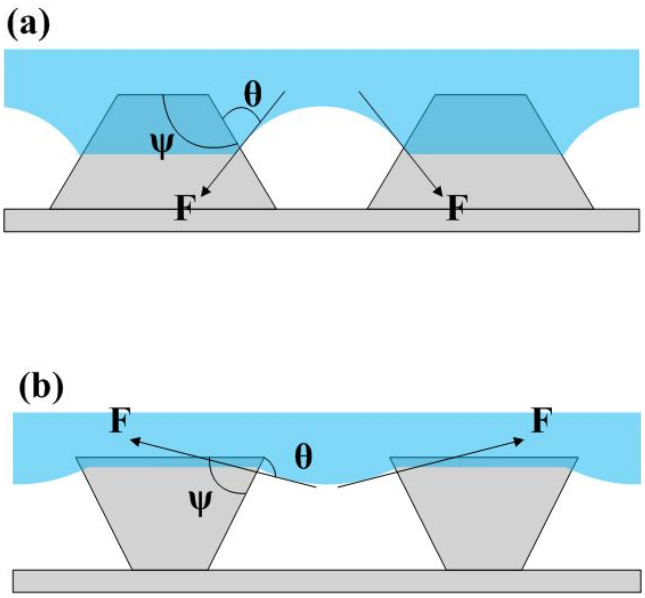


**Figure 2.4** Schematic diagrams of liquid-vapor inter face on different structures [4]

# Chapter 3

# Electrodeposition

## 3.1 Fundamental concepts

Electrodeposition refers to a film growth process which consists in the formation of a metallic coating onto a base material occurring through the electrochemical reduction of metal ions from an electrolyte. The electrolyte is an ionic conductor, where chemical species containing the metal of interest are dissolved into a suitable solvent or brought to the liquid state to form a molten salt. The

electrodeposition process consists essentially in the immersion of the object to be coated in a bath containing the electrolyte and a counter electrode, followed by the connection of the two electrodes to an external power supply to make current flow possible. The substrate to be coated is connected to the negative terminal of the power supply, in such a way that the metal ions are reduced to metal atoms, which eventually form the deposit on the surface. A general reaction of metal formation is the following:

$$M^{z+}_{solution} + ze \rightarrow M_{lattice}$$

The dissolved ions $M^{z+}$ are reduced by the electrodeposition process in which z electrons are provided by an external power supply. The schematic of electrodeposition of copper on substrate in a copper sulfate bath is shown in Figure 3.1.

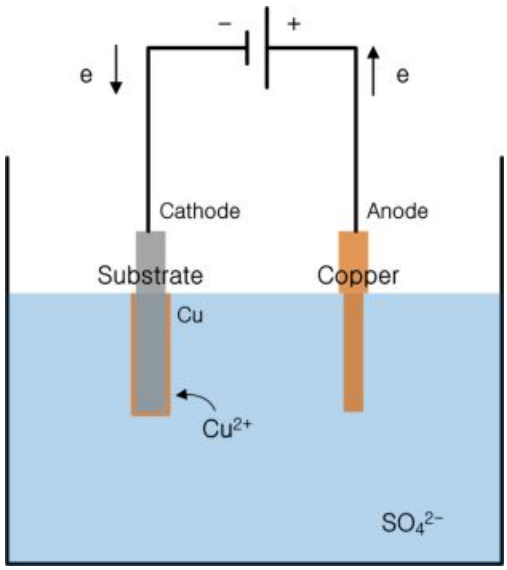


**Figure 3.1** Schematic of electrodeposition of copper on substrate in a copper sulfate bath

## 3.2 Deposition of copper

Copper is widely utilized in electrodeposition by the fact that it is a relatively inexpensive metal and also has the very useful feature that it can be deposited on top of various substrates with little technological difficulties. Copper has the highest electrical conductivity and thermal conductivity besides silver. As a metal, it is environmentally non-hazardous. The waste treatment of copper electrolytes is in most case simple and the copper metal can be recycled.

Three types of solutions are in common use such as acidic, alkaline and pyrophosphate baths. Acidic copper baths are simple in composition, stable and easy to control. They have high current efficiency and can tolerate high current density. A sulfuric acid improves solution conductivity and enhances throwing power. Alkaline solutions have much better throwing power than acidic ones.

However, solution control is more difficult, and operating current density is lower. The main drawback of these solutions is that they are toxic, requiring special care during operation as well as an expensive and well documented waste treatment process.

Electrodeposition of copper is widely utilized in various fields. In case of the IC fabrication, since 1997 it has been used for the production of interconnection lines down to 0.20 μm width. Electrochemical metal deposition methods represent a very attractive alternative to the conventional IC fabrication processes [17]. Besides, it had been applied to the fabrication of complex three-dimensional electrodes for micro electrical discharge machining that is an important issue in the field of micromachining. The electrodes was able to have various structures and surfaces by electrodeposition condition shown in Figure 3.2 [18]

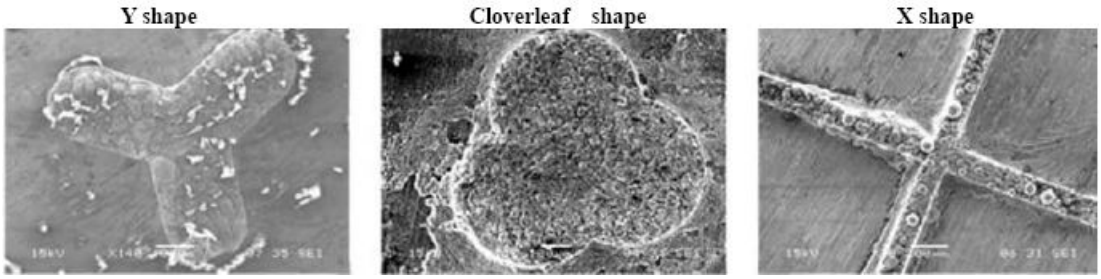


**Figure 3.2** SEM images of electrodes deposited by the local electrochemical deposition process [18]

## 3.3. Morphology

The deposit surface almost always develops a roughness pattern which may take the form of regular geometric patterns, surface undulations with well-defined amplitude and frequency, and random surface perturbations with a range of spacing, sizes and shapes. Evolution of surface irregularities is affected by substrate, active nucleation sites, competing nucleation and growth mechanisms, electrolyte, deposition conditions, crystallographic faceting and deposit defect structure [19, 20]. The key to the development of surface morphology is instabilities on the deposit surface that are intensified by mass transfer conditions near the deposit surface. Under unfavorable conditions in mass transfer, irregular growth and repeated branching structures may be observed. Controlled growth morphology can be achieved through faceting, twinning, additives, or deposition

parameters. In other words, controlling the deposition parameter such as current density can be a simple method for diversifying the surface morphology.

# Chapter 4

# Fabrication process for re-entrant structure

## 4.1 Experimental setup

The experimental setup for the fabrication process consists of a pulsed laser system for micro structuring and an electrodeposition system for re-entrant and surface structuring as shown in Figure 4.1. The micro-patterned surface of stainless steel was produced through laser ablation using a Yb-doped pulsed fiber laser (IPG photonics, YLP-C series) with a wavelength of 1064 nm and a pulse

length of 100 ns at repetition rates ranging from 20 kHz to 80 kHz. Further, the cathodic deposition of copper on stainless steel was performed in an electrochemical cell. To control the current density during electrodeposition, galavanostat (potentiostat / galvanostat model 263A from AMETEK) was used. A stainless steel (AISI 304) plate with a thickness of 500 μm was used as a workpiece. The counter and reference electrodes were 99.9% copper rods. The electrolyte for the copper electrodeposition was an aqueous solution of 0.5 M copper sulfate pentahydrate and 0.5 M sulfuric acid. The characteristics of the fabricated structure were studied using a scanning electron microscope (SEM) and contact angle analyzer (Phoenix 150 from S-EO) with 3 μl pendant drop of deionized water.

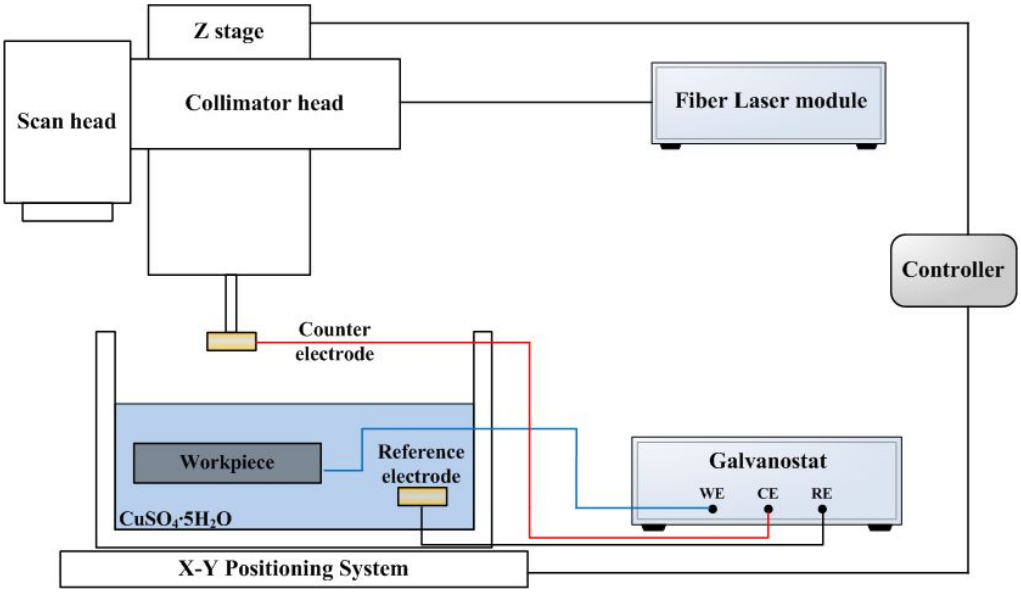


**Figure 4.1** Schematic of experimental setup for

laser ablation and electrodeposition

## 4.2 Fabrication process

The fabrication method of a metallic re-entrant structure requires the sequential process of laser ablation, insulating, mechanical polishing and electrodepostion. Its schematic process is shown in Figure 4.2. Primarily, a nanosecond pulsed laser that has a high ablation rate is used to machine a micro structure on workpiece. Subsequently, insulating material, such as enamel, is spread on the fabricated area. After insulating, the insulating material applied on the top of the micro structure is eliminated by additional mechanical polishing. The re-entrant structure is electrochemically deposited on the area exposed by polishing. Finally, insulating material is removed by ultrasonic cleaning with acetone.

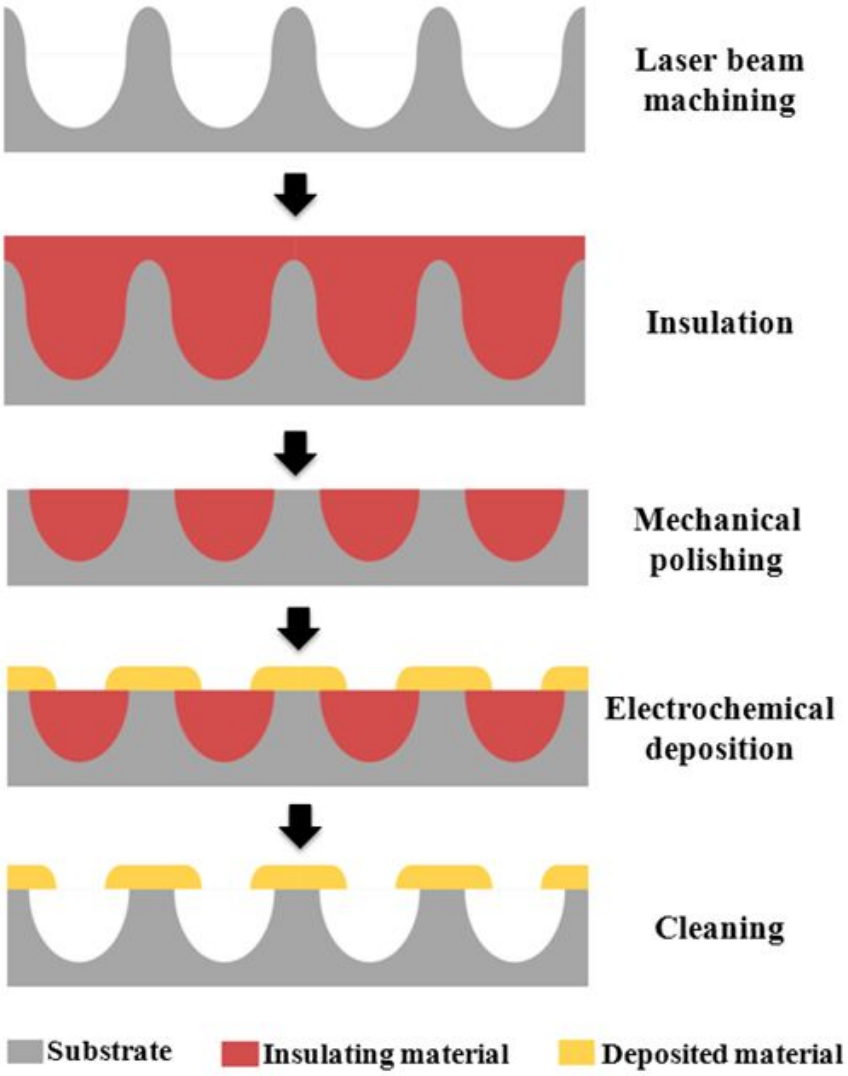


**Figure 4.2** Schematic of the sequential fabrication process

Laser ablation is an optical-thermal based machining process that is applicable to any material that absorbs light. Laser ablation using an ultra-short pulsed laser at a specific picosecond of femtosecond pulse rate can attain high-precision machining because of the short pulse duration. However, long machining time and the expense to purchase and maintain the required equipment are barriers to applying the method in industry. However, a short pulsed laser at a specified nanosecond or microsecond pulse rate enables a high ablation rate on a micro scale [21]. In a recent study, fabrication of a micro-pin array using a nanosecond pulsed laser beam was studied [22]. In this study, a micro pillar array was fabricated using a nanosecond pulsed laser beam.

When a laser beam is irradiated on a workpiece following a scanning path, as shown in Figure 4.3(a), the irradiated area with overlapped scan path is effectively ablated. Repeating the laser scanning, the micro pillar array could be fabricated as shown in Figure 4.3(b). The laser ablation conditions were set an average of 6 W of power, 80 kHz repetition rate, 9.8 mm/s scan speed, and 60 times. According to

the laser ablation conditions, a higher ablation rate makes the diameter and height of the pillars smaller and a lower ablation rate creates larger pillars. In Figure 4.3, the scanning path and fabricated structure of a micro pillar array resulted in 280 μm spacing of the pillars. Changing the number of overlapped scan lines will cause the spacing of the micro pillar array to create an effect on the water contact angle because of the contact area between the water droplet and the structure.

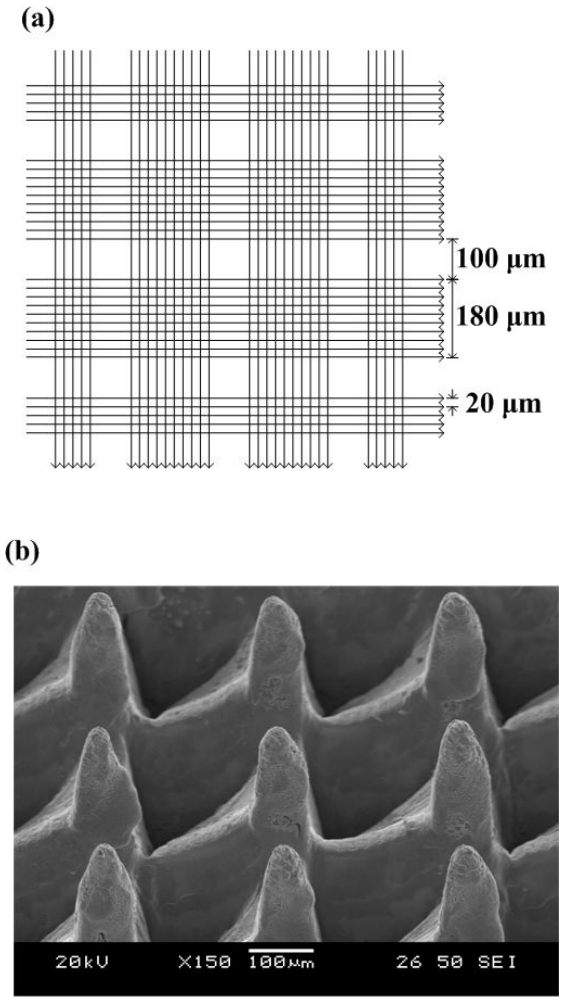


**Figure 4.3** Micro pillar array fabricated by laser ablation in 280 µm spacing; (a) scanning path (b) SEM image at 45˚ tilt angle

To fabricate the template for electrochemical deposition, the additional processes of insulating and mechanical polishing were performed after the laser ablation. The micro-structured surface is filled with insulating material. In this case, enamel was used. Enamel has an electrical resistivity and is easily cleaned with a solvent such as an acetone. Subsequently, the insulated surface was polished with sand paper. Electrochemical reaction is restricted on a surface unsheltered by mechanical polishing. After the electrodeposition, copper was deposited on the micro pillar array. The insulating material was cleaned from the surface using ultrasonic vibration with acetone. Finally, a re-entrant structure array could be fabricated through laser ablation and electrodeposition as shown in Figure 4.4. Different wetting phenomena between re-entrant structure array and flat surface were shown in Figure 4.5.

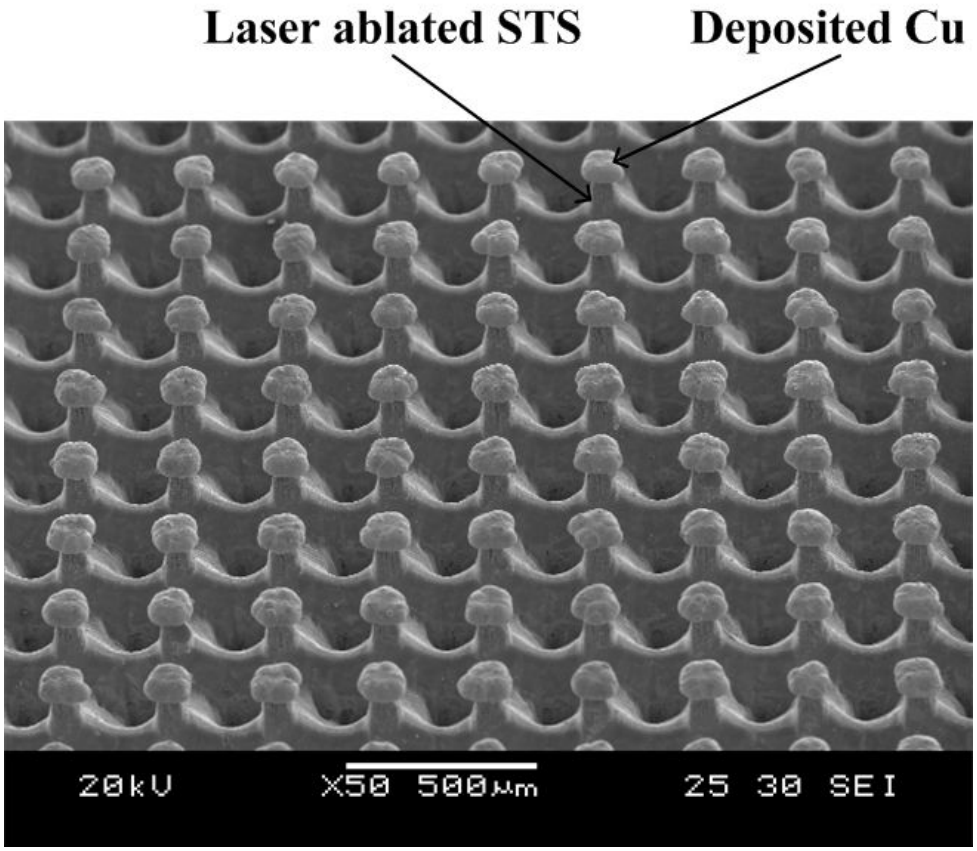


**Figure 4.4** SEM image of the re-entrant structure array after electrodeposition at 45˚ tilt angle; laser ablation created 280 µm spacing of pillars and electrodeposition was accomplished at a current density of 640 µA/mm$^2$

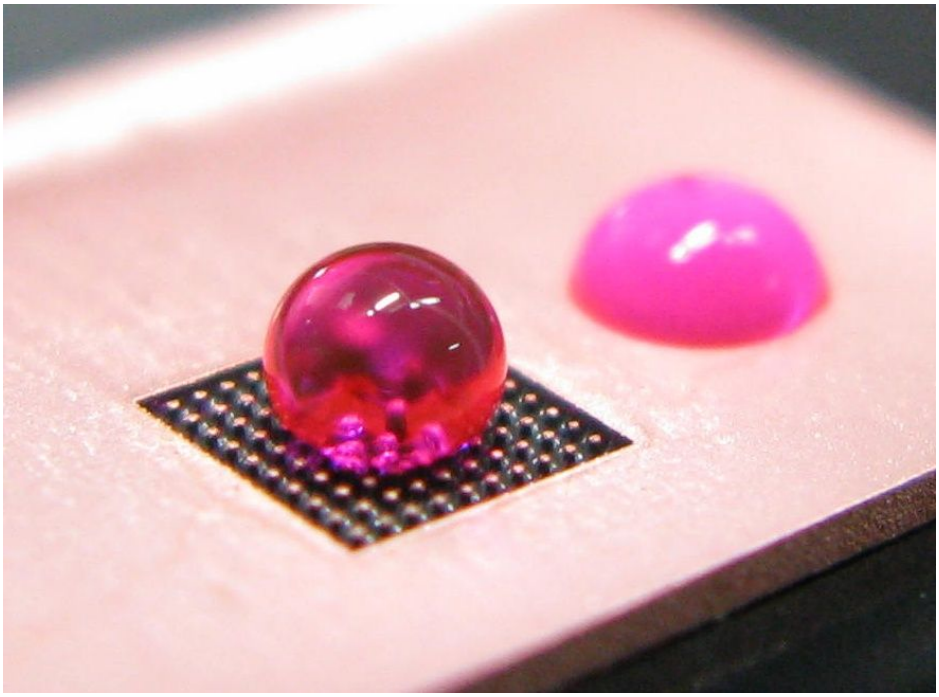

**Figure 4.5** CCD image of water droplets on the re-entrant structure array and flat surface; laser ablation created 280 μm spacing of pillars and electrodeposition was accomplished at a current density of 640 μA/mm$^2$

When the liquid droplet is on the surface, the force generated by the liquid droplet is toward upward because of the smaller local texture angle than water contact angle, shown in Figure 4.6. The re-entrant structure can play an role to repel the water. The practical local texture angle of fabricated structure can be considered zero because continuous line from deposited material to pillar of substrate has a horizontal line shown in Figure 4.7.

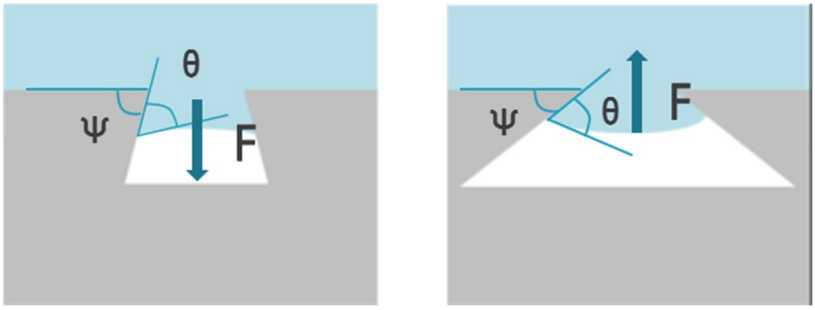


(a) (b)

**Figure 4.6** Schematic of liquid droplet on different local texture angle (a) local texture angle ψ < water contact angle θ and (b) local texture angle ψ > water contact angle θ

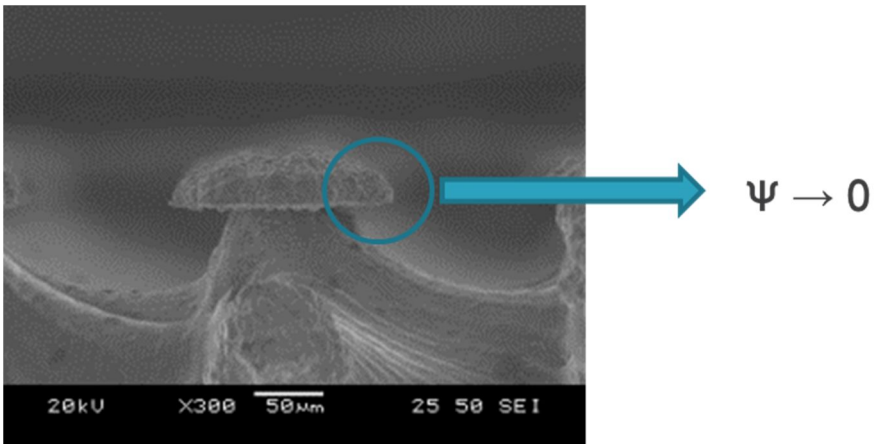


**Figure 4.7** SEM imager of fabricated re-entrant structure (side view)

In the fabrication process of manufacturing a super-hydrophobic surface, the surface morphology formed by the spacing of the micro pillar array and electrodeposition is important. Using the proposed fabrication process, a 3 mm by 3 mm patterned surface was fabricated at specific micro pillar spacing in the arrays at three current densities during electrodeposition. The product of current density and the electrodeposition process time were controlled in order to sustain the amount of deposited copper. In general, the amount of electrodeposition is approximately proportional to the current density and time as defined by Faraday's law. In this experiment, the main consideration was the water contact angle relative to the surface morphology of deposition. Figure 4.8 shows the SEM images and water contact angles of the fabricated structure.

| Spacing | Current Density | | |
|---|---|---|---|
| | 320 μA/mm$^2$ | 640 μA/mm$^2$ | 1280 μA/mm$^2$ |
| 180 μm | 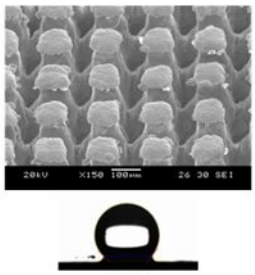 130° | 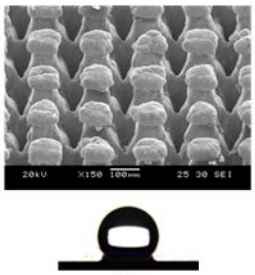 128° | 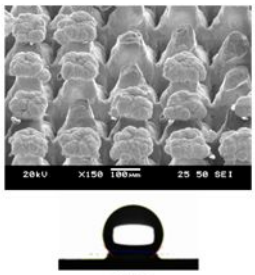 119° |
| 280 μm | 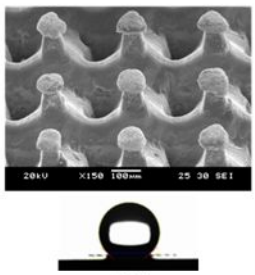 133° | 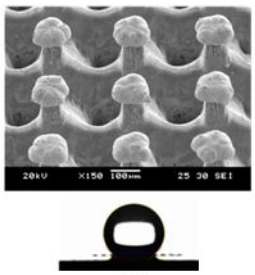 132° | 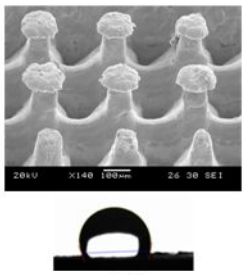 104° |
| 380 μm | 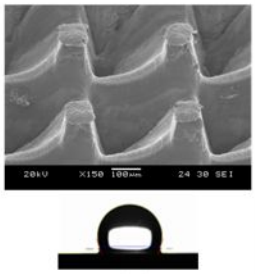 105° | 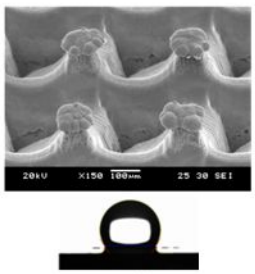 119° | 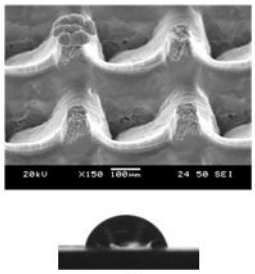 72° |

**Figure 4.8** SEM image and water contact angle of micro pillar arrays fabricated using electrodeposition at the noted current densities (320 μA/mm$^2$ for 1 hour, 640 μA/mm$^2$ for 30 min, 1280 μA/mm$^2$ for 15 min) and spacing (180 μm, 280 μm, 380 μm); error range of water contact angles was ±1˚.

## 4.3 Water contact angle relative to the spacing of the micro pillar array

A droplet resting on a solid surface and surrounded by a gas forms a characteristic contact angle. If the solid surface is rough, and the liquid is in intimate contact with the solid asperities, the droplet is in the Wenzel state. If the liquid rests on the tops of the asperities, it is in the Cassie-Baxter state. The Wenzel or Cassie-Baxter state can be predicted by the minimization of free energy argument [23].

In this research, the wetting state was assumed to be in the Cassie-Baxter state. Supposing the wetting state was a Wenzel state, the surface should be more hydrophilic in nature because the ratio of the actual area to the projected area is very large relative to the re-entrant structure. On the other hand, hydrophobicity of fabricated surface with re-entrant structure array was increased compared to that

of deposited flat surface. In the Cassie-Baxter state, the liquid contact with a composite surface of solid and air is described by the Cassie-Baxter equation.

Fractional surface areas: $f_1$, $f_2$

$\gamma_{SL}$: Solid-liquid surface tension

$\gamma_{LV}$: Liquid-vapor surface tension

$\gamma_{SV}$: Solid-vapor surface tension

$\theta$: Contact angle of flat surface

$\theta^*$: Contact angle of structured surface

$$dF = f_1(\gamma_{SL} - \gamma_{SV})_1 dx + f_2(\gamma_{SL} - \gamma_{SV})_2 dx + \gamma_{LV}\cos\theta^* = 0$$

$$\cos\theta^* = f_1\cos\theta_1 + f_2\cos\theta_2$$

In the case of a fabricated structure, fractional surface area $f_1$ is the top surface of the re-entrant structure and $f_2$ is air, with a water contact angle of 180˚. Therefore, the fabricated surface with greater micro pillar spacing had a larger contact angle and shows a more hydrophobic surface. In Figure 4.8, at a current density of 320 μA/mm$^2$ and 640 μA/mm$^2$, the structure fabricated at 280 μm spacing shows a larger water contact angle than that fabricated at 180 μm spacing. On the other hand, the structure fabricated at 380 μm spacing shows a smaller contact angle because the spacing was too large to form the water droplet on the top surface of the structure. Consequently, the water droplet permeated the spacing of the structure. The drooping water droplet resulted in an increased contact area between the water droplet and the structure. The experimental values were compared to theoretical values of Cassie-Baxter model and Wenzel model shown in Figure 4.9. The water contact angles of the structures fabricated at 180 μm spacing were within the range of theoretical values of Cassie-Baxter model. The larger the spacing of micro pillar, the experimental values were approached to the theoretical values of Wenzel model. Based on this result, the experiment

incorporated a gradual increase of current density, as discussed in the next section, and the fabricated structure with 280 μm spacing was used.

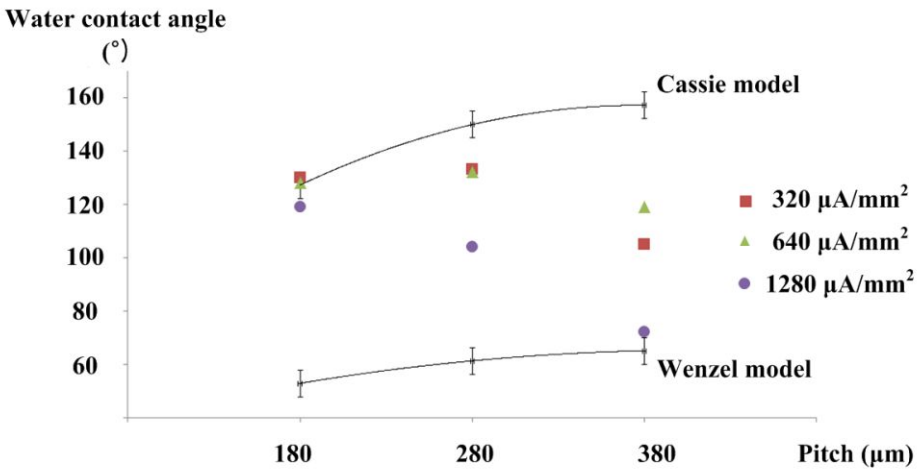


**Figure 4.9** Comparison between theoretical values (Cassie model and Wenzel model) and experimental values

## 4.4 Water contact angle relative to current density in electrodeposition

Surface morphology of the deposited surface changed relative to the current density during electrodeposition, as shown in Figure 4.10. A higher current density creates a surface that is more rugged and rough. The average roughness, Ra, was 0.408 μm at 320 μA/mm$^2$ and was 4.131 μm at 1280 μA/mm$^2$. The topography of deposited copper was altered by electrodeposition conditions such as the electrical condition, electrolyte, hydrogen evolution, etc [19, 20].

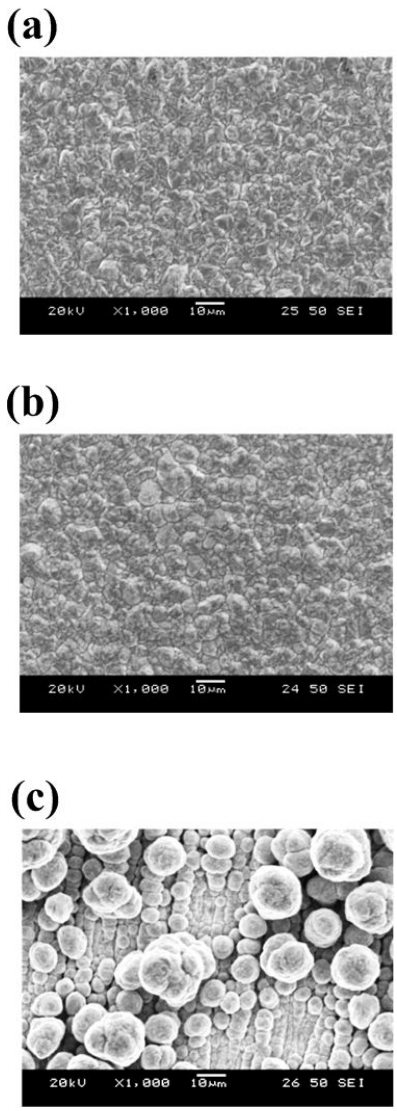


**Figure 4.10** SEM image of surface fabricated by electrodeposition relative to current density (a) 320 μA/mm$^2$, (b) 640 μA/mm$^2$ and (c) 1280 μA/mm$^2$

During the fabrication process, the electrodeposition process was carried out using current densities of 320 μA/mm$^2$, 640 μA/mm$^2$ and 1280 μA/mm$^2$. As shown in Figure 4.8, an increase in the current density resulted in a more rugged surface morphology across the entire range of spacing. Although the surface became more rugged as current density increased, it also had a small effect on the water contact angle at current density of 320 μA/mm$^2$ and 640 μA/mm$^2$ (Figure 4.8). At a current density of 1280 μA/mm$^2$, the highest current density used in the experiment, loss of deposited copper occurred. The ruggedness of deposited morphology and the adhesion problem of the deposit and substrate are related to the metal ions in the boundary layer.

During the electrochemical reaction, the concentration of metal ions in the electrical double layer near the cathode is reduced with respect to the bulk concentration. Distribution of ions inside the electrical double layer is determined by diffusion. With increasing current density, the metal ions are eventually depleted near the surface and the current is limited by the diffusion of ions. Thus,

at higher current densities near the limiting current, the electrodeposition is governed by a diffusion-limited non-local mechanism. The surface morphology becomes unstable and bulk-fractal-like microstructures such as dense-branching and dendritic patterns [19]. Likewise, adhesion of deposited copper to the substrate weakens at a higher current density. At the initial stage of electrodeposition, once the nuclei are formed, the adatom clustering grows rapidly, forming a bumpy structure of growth centers. At a higher current density, the bulk deposit spreads laterally across the substrate surface [20]. Consequently, coarsening of the structure leads to weak adhesion.

For above reasons, the study considered a gradual increase of the current density. Control of the current densities (from low to high) results in a fabricated surface with good adhesion of deposit to substrate and a higher roughness of the deposited surface. The experimental conditions are shown in Table 4.1. The total product of current density and time was maintained in order to adjust the amount of copper deposited. The proportion of deposition in each step of the overall

process is stated within parentheses in Table 4.1, (the amount of deposition in each step/total amount of deposition). While controlling the amount of electrodeposition at each level of current density, the surface morphology and water contact angle were observed. When the fraction of deposition at the highest current density (1280 $\mu A/mm^2$) increased, the deposited morphology became a dendritic structure. As the electrodeposition progresses, copper deposited on a dendritic structure reduces the robustness of the structure. Under the experimental condition shown in Figure 4.11(c), although the electrodeposition was initiated at the lowest current density (320 $\mu A/mm^2$), the deposited fraction at the highest current density was chipped off. Consequently, the deposited copper played a role in increasing surface roughness of the structure. The surface became more hydrophilic, with an 8˚ water contact angle. The droplet was in the Wenzel state. On the other hand, Figure 4.11(e) and (g) illustrate low current density experimental sets (e) and (g) where the deposited surface was smooth compared to other conditions. Water contact angles were not much different relative to current density due to the unsatisfactory variance in the ruggedness of the surface. In

experimental set (d), the same fraction of electrodeposition was made at each step and the deposited surface had a greater roughness, maintaining structure robustness. It resulted in a super-hydrophobic surface and a 153˚ water contact angle due to the formation of a more composite solid-liquid-air interface.

**Table 4.1** Experimental conditions of electrodeposition with a gradual increase in current density; fractional numbers in parenthesis refer to the proportion of deposition in each step of the overall process.

| Experimental set | Current density | | |
|---|---|---|---|
| | 320μA/mm$^2$ | 640μA/mm$^2$ | 1280μA/mm$^2$ |
| (a) | 0 min (0) | 10 min (1/3) | 10 min (2/3) |
| (b) | 0 min (0) | 20 min (2/3) | 5 min (1/3) |
| (c) | 20 min (1/3) | 0 min (0) | 10 min (2/3) |
| (d) | 20 min (1/3) | 10 min (1/3) | 5 min (1/3) |
| (e) | 20 min (1/3) | 20 min (2/3) | 0 min (0) |
| (f) | 40 min (2/3) | 0 min (0) | 5 min (1/3) |
| (g) | 40 min (2/3) | 10 min (1/3) | 0 min (0) |

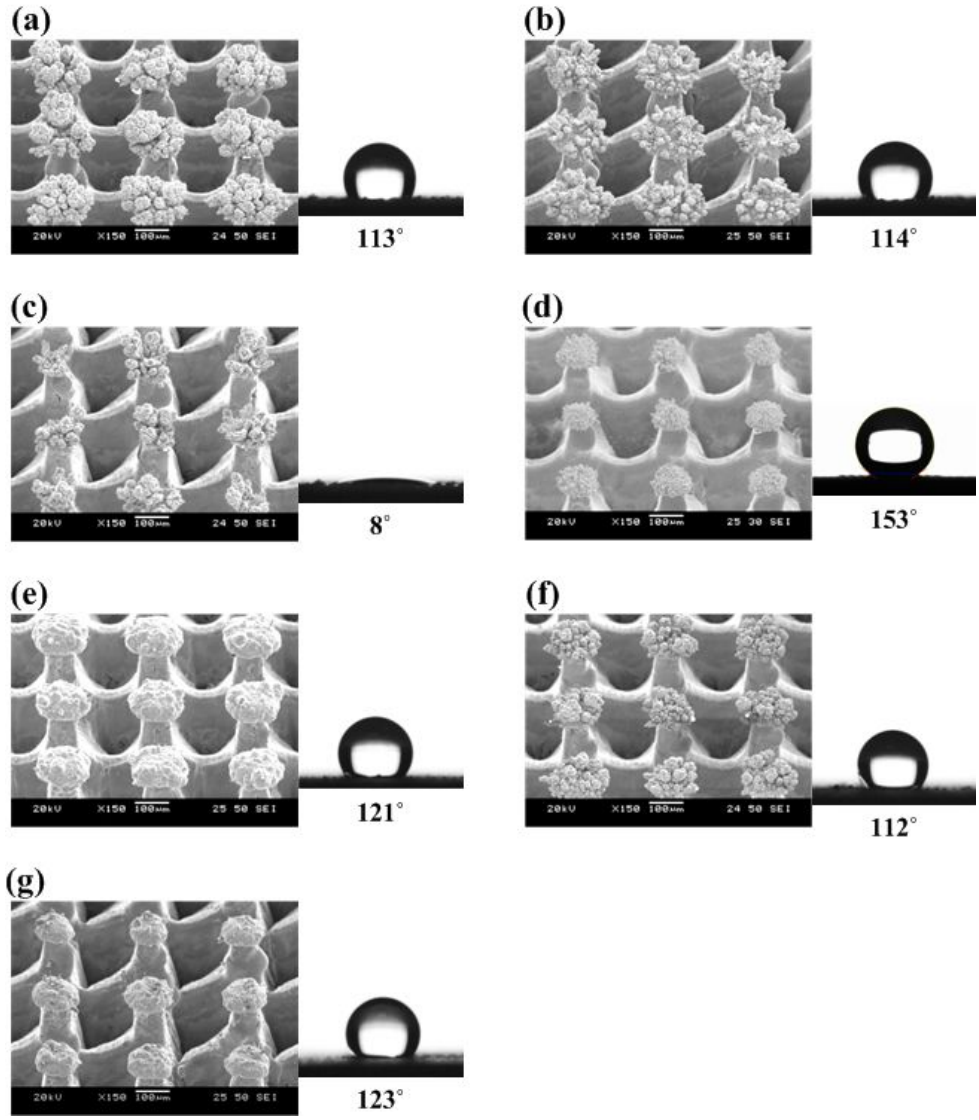


**Figure 4.11** SEM image and water contact angle of micro pillar array fabricated using electrodeposition with a gradual increase in current density; experimental conditions are noted in Table 4.1

## 4.5 Material combinations of substrate and deposited material

Material combinations of Substrate and deposited material were investigated. To confirm the effectiveness of sequential process of laser ablation, insulation, mechanical polishing and electrodeposition to other material combinations, nickel deposition on stainless steel and copper deposition on copper were carried out. SEM images and water contact angles of fabricated re-entrant structure arrays were shown in Figure 4.12. Hydrophobic surfaces of re-entrant structure arrays with nickel deposition on stainless steel and copper deposition on copper were successfully fabricated. These results shows sequential fabrication process can be utilized for various materials. In order to fabricate the super-hydrophobic surfaces, it is necessary to study on parameters of electrodeposition process, the same as

copper deposition on stainless steel in this research.

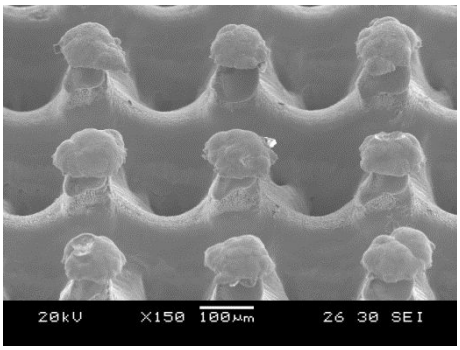


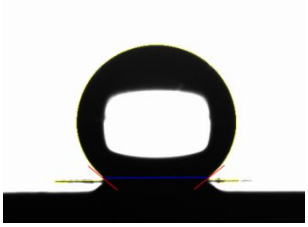

**138°**

(a)

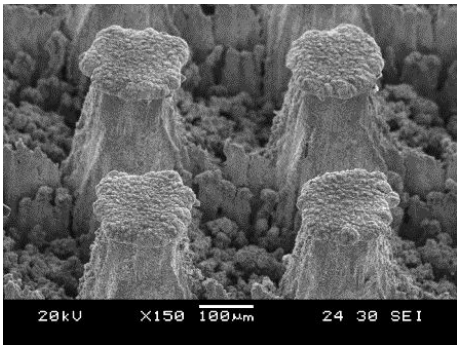


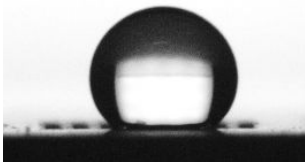

**119°**

(b)

**Figure 4.12** SEM image and water contact angle of re-entrant structure array fabricated using sequential process including laser ablation, insulation, mechanical polishing and electrodeposition; (a) nickel deposition on stainless steel and (b) copper deposition on copper

# Chapter 5

# Fabrication process for hierarchical structure

## 5.1 Fabrication process

Surface morphology of the deposited surface changed relative to the current density during electrodeposition, as shown in Figure 4.10 of previous chapter. Although an increase in the current density resulted in a more rugged surface morphology across the entire range of the current densities, the surfaces were hydrophilic (water contact angle < 90˚). However, the deposited surface under

current density of 2560 μA/mm$^2$ was a hydrophobic, shown in Figure 5.1 (d). Using the hydrophobicity of deposited surface, fabrication method of a super-hydrophobic surface can be simplified compared to fabrication process for re-entrant structure. The hydrophobicity of surface is governed by physical structure and surface energy. It is described in next sections, 5.2 and 5.3.

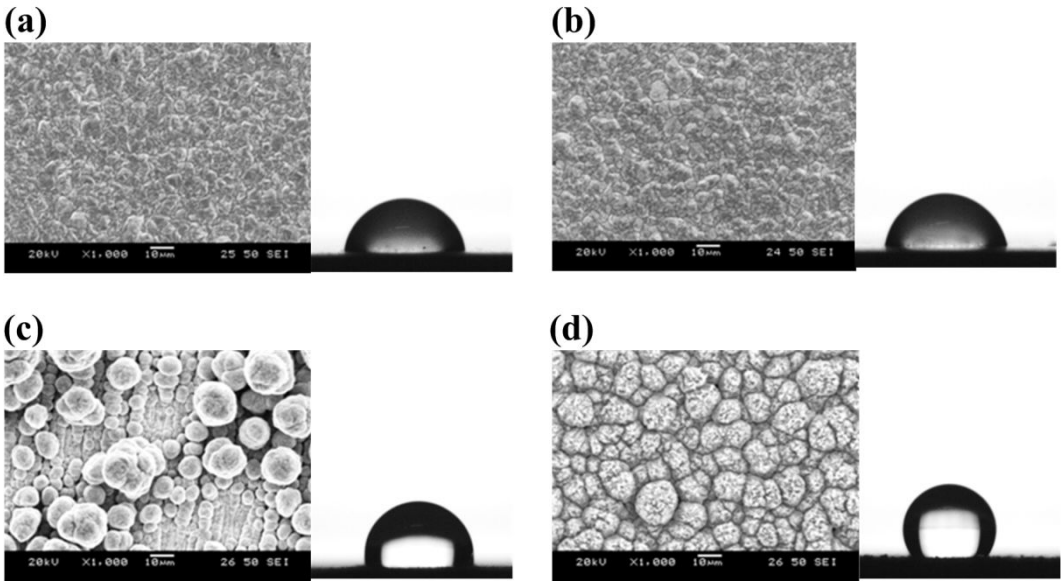


**Figure 5.1** SEM image and water contact angle of surface fabricated by electrodeposition relative to current density (a) 320 μA/mm$^2$, (b) 640 μA/mm$^2$ , (c) 1280 μA/mm$^2$ and (d) 2560 μA/mm$^2$

The fabrication method of a super-hydrophobic surface for hierarchical structure requires the machining process for micro structure and electrodeposition. In this research, laser ablation was used for micro structure. However, it can be replaced with some other machining process such as mechanical machining, electrical discharge machining and electrochemical machining. Schematic process is shown in Figure 5.2. Fabricated super-hydrophobic surface was shown in Figure 5.3. Primarily, a nanosecond pulsed laser that has a high ablation rate is used to machine a micro structure on workpiece. Subsequently, the electrodeposition was performed. In this fabrication process, substrate was the same as deposit material because the excessive current density was applied. In the case of deposition on the other material combinations, adhesion problem between substrate and deposit can be easily occurred.

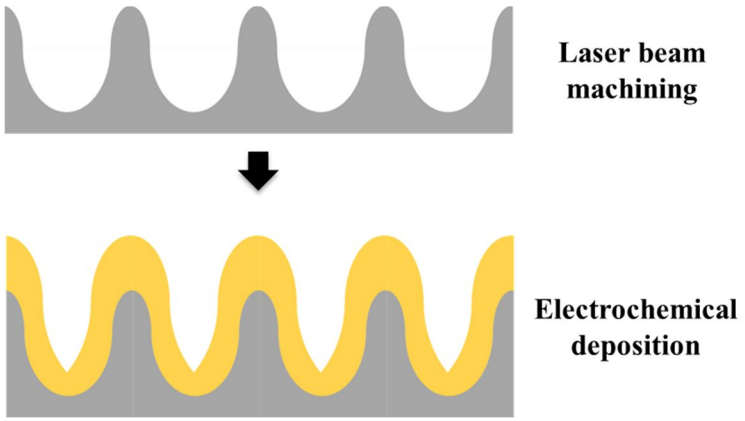


**Figure 5.2** Fabrication process for hierarchical structure

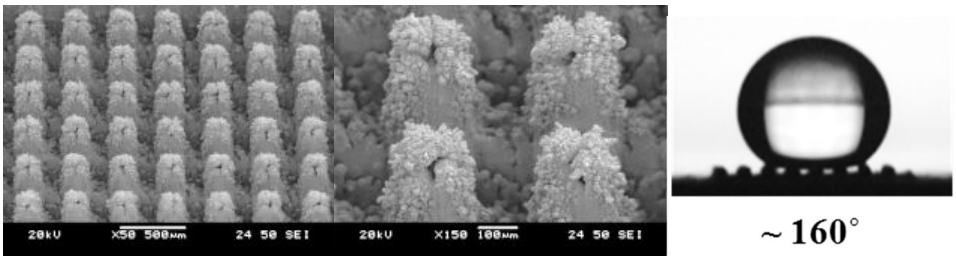


**Figure 5.3** SEM image and water contact angle of fabricated surface using fabrication process for hierarchical structure

## 5.2 Effect of copper oxide

To investigate the characteristics of deposited surface, X-ray diffractometry (XRD) was performed. XRD analysis provides the information on phase identification and preferred crystal orientations. Figure 5.4 shows the XRD patterns of deposited surfaces. The surfaces have copper peaks in common and comparatively difference in preferred crystal orientations. The preferential orientation of hydrophilic surface (deposited surface under current density of 640 $\mu A/mm^2$, Figure 5.4(a)) was (220) direction. On the other hand, (220) direction of hydrophobic surface (deposited surface under current density of 2560 $\mu A/mm^2$, Figure 5.4(a)) was degraded. Although preferred crystal orientations of surface can have an effect on surface energy, there are no significant differences between

the number of broken bonds in (220) plane and (111) plane. It has little effect on hydrophobicity of surface.

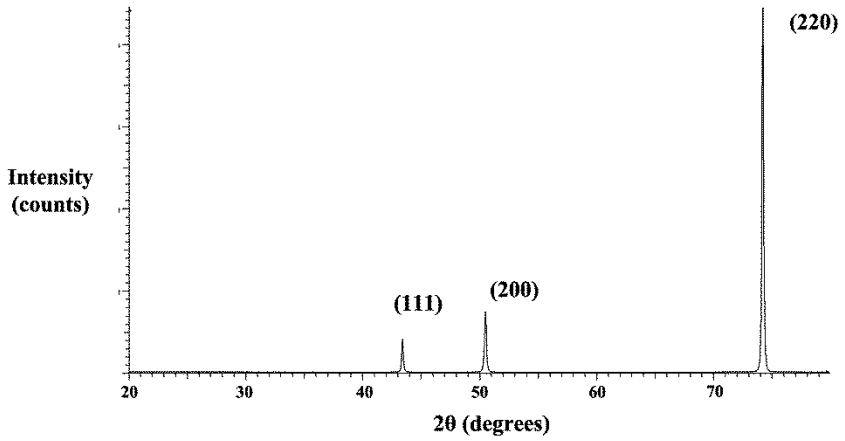


(a)

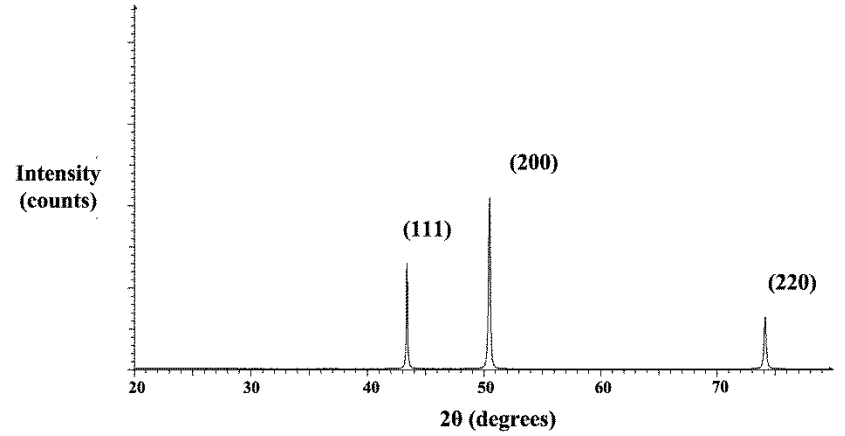


(b)

**Figure 5.4** XRD patterns of deposited copper surface: (a) current density: 640 $\mu A/mm^2$ and (b) 2560 $\mu A/mm^2$

To investigate the effect of copper oxide, copper oxidation tests on flat surfaces and structured surfaces were carried out. At first, copper surfaces without structure were heat treated for 20 minutes at specific temperatures. The surface property was analyzed by SEM, CCD, water contact angle and XRD shown in Figure 5.5. Surface morphology was obserbed by SEM image. Copper (I) oxide, brownish-red solid and copper (II) oxide, black powder surface were distinguished by color on CCD image. Wettability and chemical composition was analyzed by water contact angle and XRD analysis.

The water contact angle of oxidized surface increased by 125° until 200 ℃, and dropped back. Fully wetting was shown at 500℃. On the copper surface oxidized at 200 ℃ which had a hydrophobicity, copper peaks were detected only while copper oxide peaks were not detected by XRD because it was too thin to detect by X-ray. Over 300 ℃, surface had a hydrophilicity and copper oxide peaks were detected by XRD. Copper surface was oxidized to powder type of hydrophilic copper (II) oxide. On the other hand, copper surface was oxidized to

hydrophobic copper (I) oxide with the temperature under 200 ℃. These are similar to the results of previous research [24]. Copper (I) oxide and Copper (II) oxide have different wettability due to different inter-particle bonds.

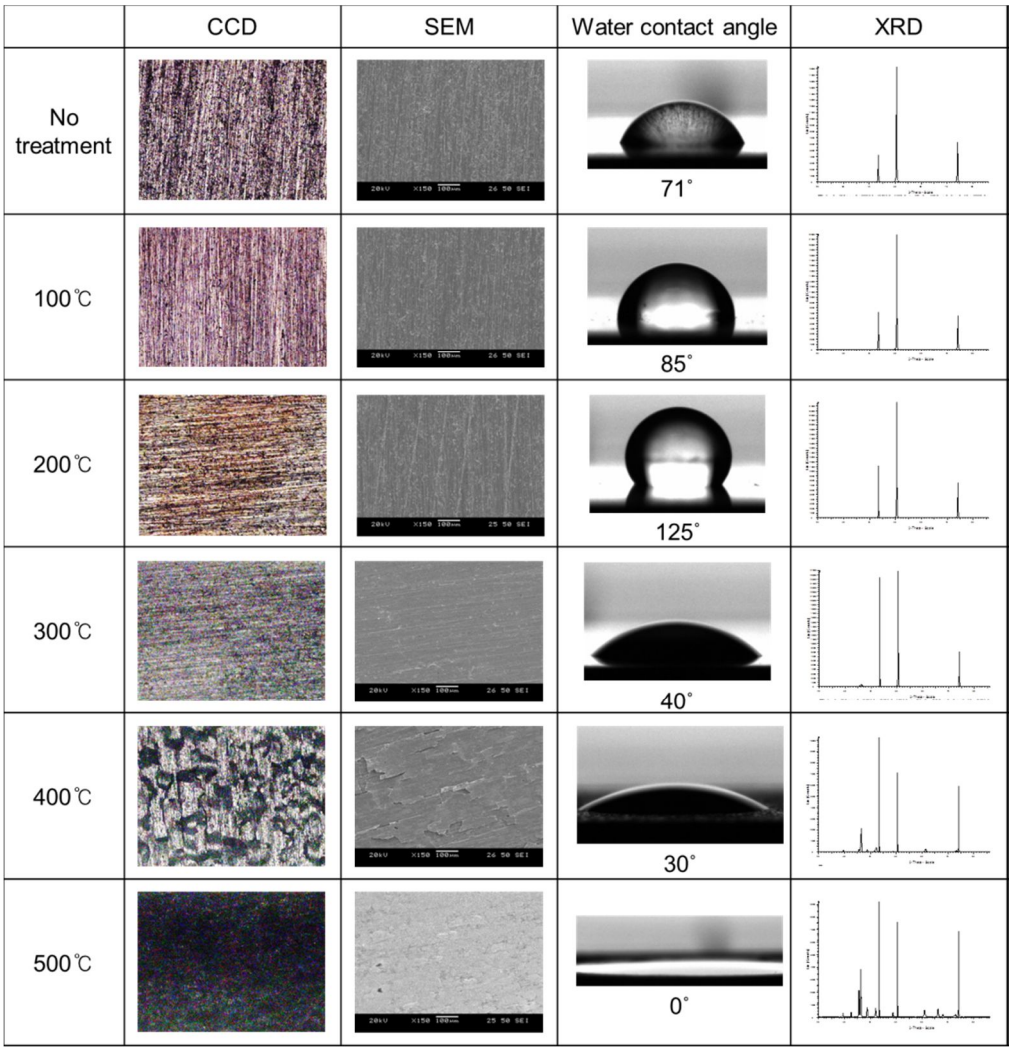


**Figure 5.5** Heat oxidized copper surfaces for 20 min; (No treatment, 100℃, 200℃, 300℃, 400℃, 500℃)

In order to clarify the effect of copper oxide, micro structures fabricated by laser ablation and mechanical polishing were oxidized by heat treatment. Laser ablation was used for fabricating micro structure and mechanical polish was used for excluding the effect of surface roughness. Micro structures were fabricated relative to the spacing of micro pillar. Copper oxidation was performed at 200 ℃ for 20 minutes. Hydrophobicity of the structured surfaces was increased by heat oxidation shown in Figure 5.6. It indicates that copper oxide contributes to hydrophobicity of surface.

| Pitch | SEM | Before oxidation | After oxidation |
|---|---|---|---|
| 180 μm | 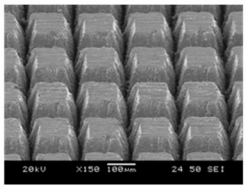 | 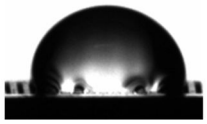 87° | 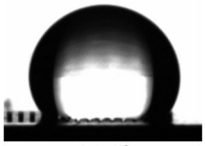 121° |
| 280 μm | 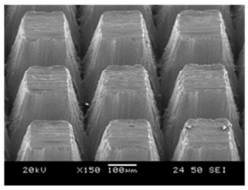 | 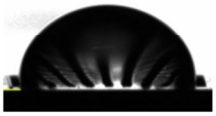 85° | 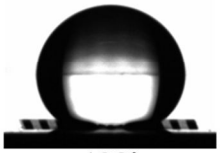 132° |
| 380 μm | 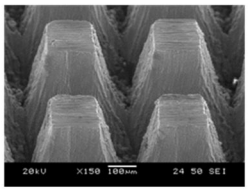 | 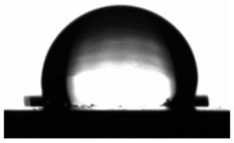 91° | 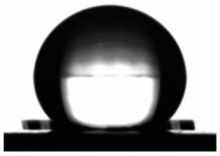 135° |

**Figure 5.6** Fabricated surface using sequential process of laser ablation, mechanical polishing and heat oxidation at 200℃

## 5.3 Effect of hierarchical structure

In order to confirm the effect of hierarchical structure, the surfaces were fabricated using sequential process of laser ablation and electrodeposition according to current density and oxidation shown in Figure 5.7. Hydrophobicity of deposited structure was increased by copper oxidation. However, the super-hydrophobicity was available on hierarchical structure fabricated at highest current density condition.

Copper oxide on the structure was removed by dipping in 0.01 M hydrochloric acid [25] for 3 minutes, shown in Figure 5.8. Although the structure was not changed by oxide removal, the water contact angle was lowered. It shows the copper oxide removal reduced hydrophobicity. In conclusion, hierarchical

structure and copper oxide were essential factors for super-hydrophobicity in the fabricated structure.

| Current | SEM | Before oxidation | After oxidation |
|---|---|---|---|
| 640 μA/mm$^2$ | 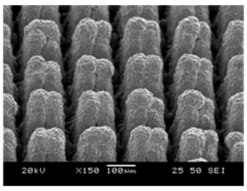 | 35˚ | 103˚ |
| 1280 μA/mm$^2$ | 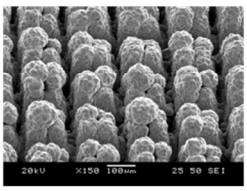 | 87˚ | 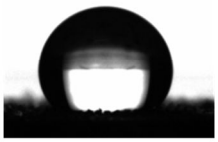 124˚ |
| 2560 μA/mm$^2$ | 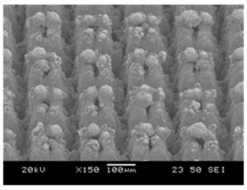 | 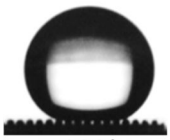 160˚ | 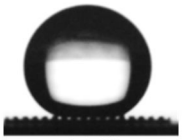 161˚ |

**Figure 5.7** Fabricated surface using sequential process of laser ablation, electrodeposition and heat oxidation at 200℃

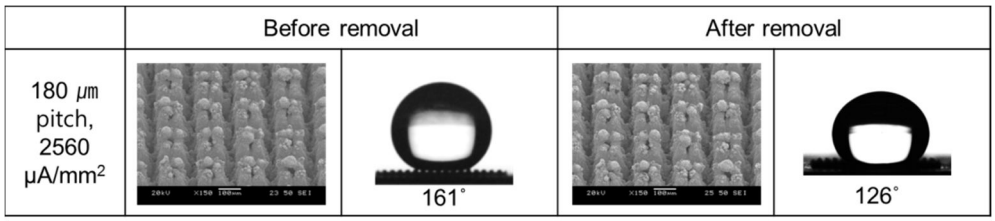


**Figure 5.8** Hierarchical structure according to copper oxide removal

## 5.4 Water contact angle relative to the depth of micro structure

To investigate the minimum requirement of depth of micro structure, the structures were fabricated relative to average depth according to number of scan in laser ablation, shown in Figure 5.9. The structures fabricated under 65 μm in average depth didn't have a super-hydrophobicity. The structures fabricated over 135 μm in average depth were super-hydrophobic surfaces.

Comparing the surface profile shown in Figure 5.10, in the case of 65 μm in average depth, depth of structure was from 50 to 80 um. In the case of 135 μm in average depth, depth of structure was from 110 to 160 um. In order to obtain the super-hydrophobic surface using electrodeposition, depth of micro structure should be above 100 μm.

Figure 5.11 shows the water contact angle relative to the spacing and depth of micro structure. When the depth of micro structure was above 100 μm, the super-hydrophobic surfaces were fabricated in the entire range of the spacing.

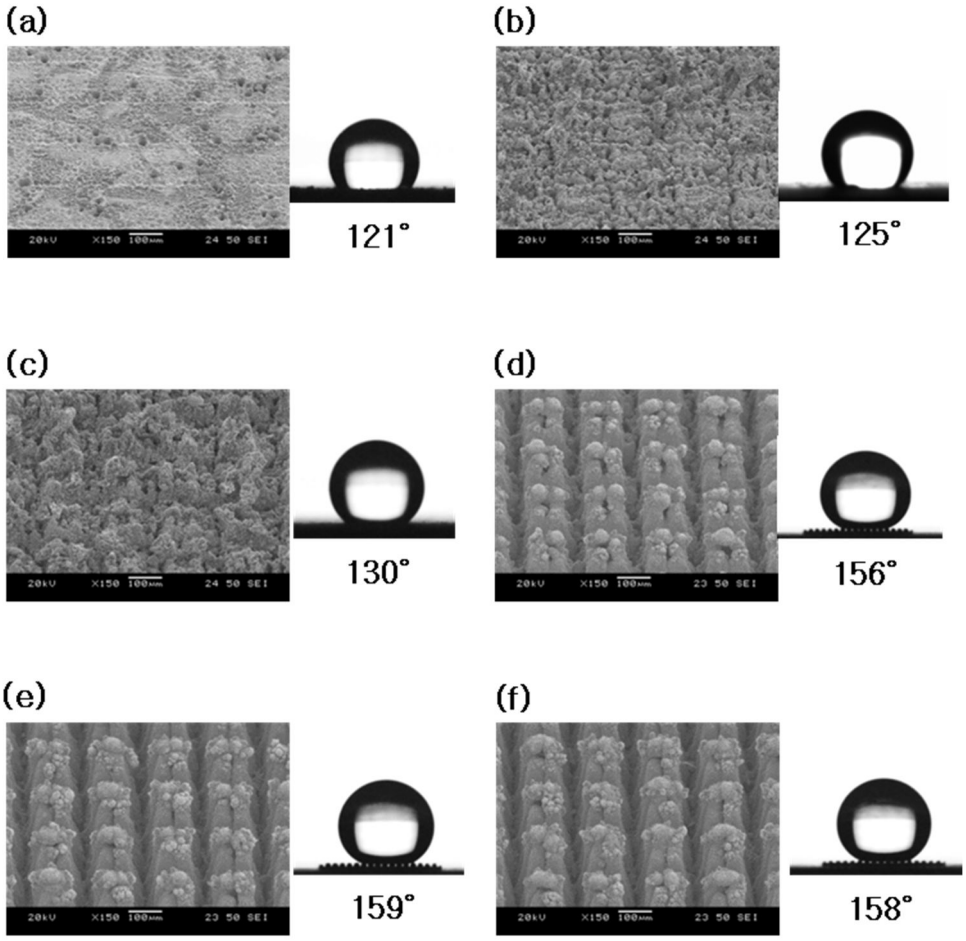


**Figure 5.9** SEM image and water contact angle of surface fabricated by fabrication process for hierarchical structure relative to average depth of micro structure (a) 10, (b) 30, (c) 65, (d) 135, (e) 200 and (f) 275 μm

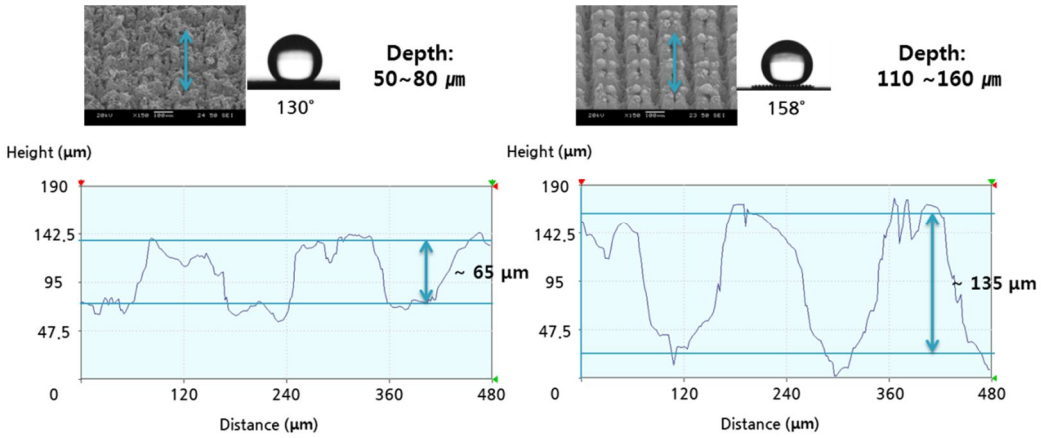


**Figure 5.10** Surface profile of surface fabricated by fabrication process for hierarchical structure: average depth (a) 65 and (b) 135 μm

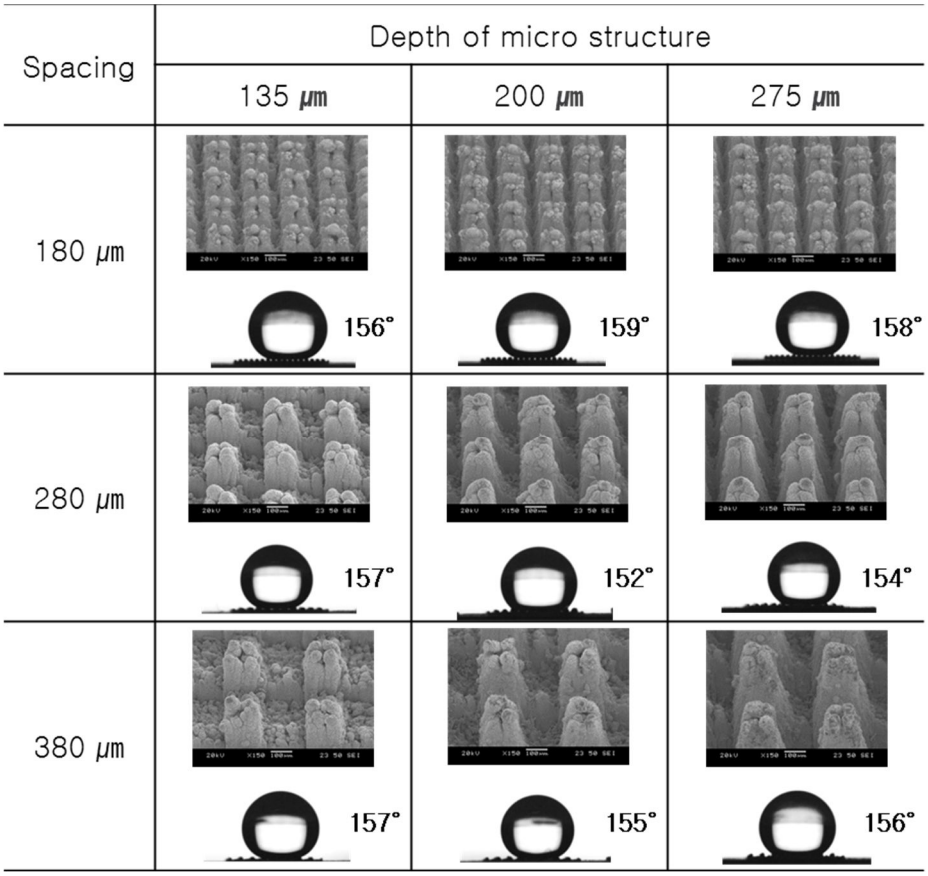


**Figure 5.11** SEM image and water contact angle of micro pillar arrays fabricated by fabrication process for hierarchical structure relative to spacing and average depth

# Chapter 6

# Dynamic robustness of hydrophobicity

To investigate the robustness of the Cassie-Baxter state liquid droplets according to the external factors, sliding test and squeezing test was carried out. In practical samples, there often exists a transitional state between Wenzel and Cassie-Baxter states, wherein surface water droplets can slide when the surface is tilted at a certain angle, so-called “roll off angle”. The sliding angle can reflect the contact angle hysteresis. As the drop is tilted, a drop place on a surface has a spectrum of contact angles ranging from the advancing contact angle to the receding contact angle. The contact angle hysteresis is defined as difference between advancing contact angle and receding contact angle. Generally, a super-hydrophobic surface

should exhibit a low contact angle hysteresis (< 10 ~ 20˚) [26]. The squeezing test was used to describe the variation of the surface state and resulting contact angle when the liquid was squeezed into the structures [27].

## 6.1 Sliding test

To investigate the roll-off angle and contact angle hysteresis, the surface fabricated using using re-entrant structure by gradual increase of current density in electrodeposition and hierarchical structure in 180 μm, 280 μm and 380 μm spacing. Test results of advancing and receding angle by the dynamic sessile drop method were shown in Figure 6.1. Sliding test results were shown in Figure 6.2 and Table 6.1.

The fabricated surface with greater micro pillar spacing had a high roll off angle and shows a higher contact angle hysteresis. Pinning effect of wetting was shown when a liquid droplet gets contact with an edge of a solid surface [28]. Smaller spacing of the micro structure is effective in terms of contact angle hysteresis.

In the case of the fabricated surface using re-entrant structure, roll off angle and contact angle hysteresis was highest in the experimental set because the intrinsical hydrophobicity of the surface was lower than that of the fabricated surface using hierarchical structure.

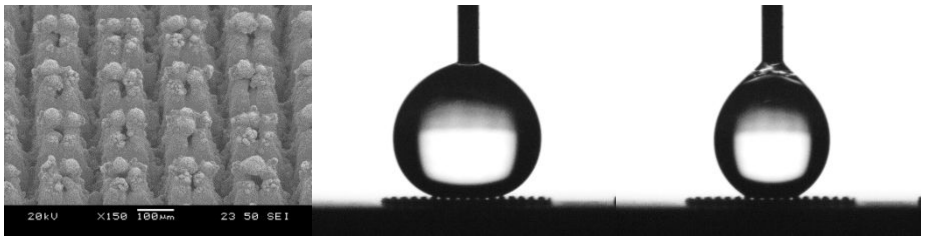


(a)

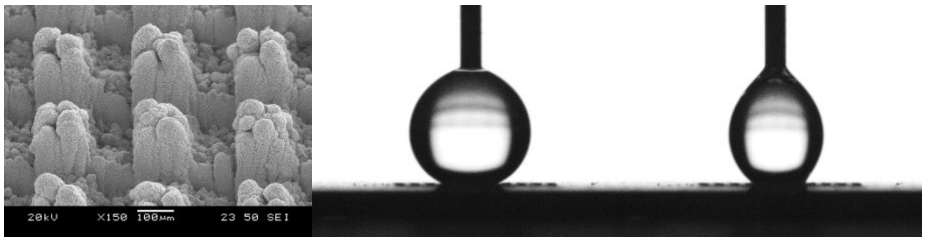


(b)

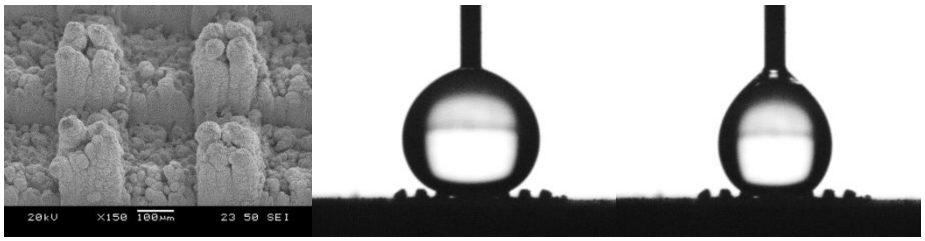


(c)

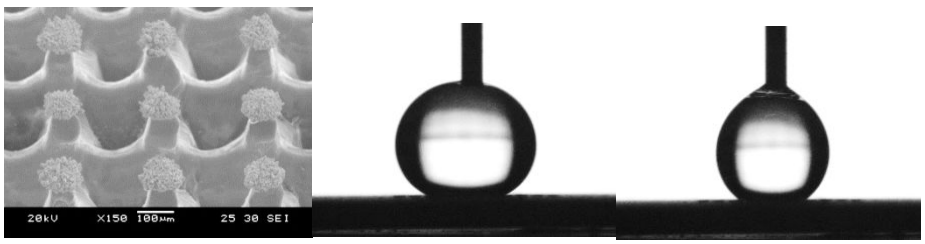


(d)

**Figure 6.1** The captured images of advancing and receding angle by the dynamic sessile drop method: fabricated structure using hierarchical structure in (a) 180 µm, (b) 280 µm and (c) 380 µm spacing, and (d) re-entrant structure

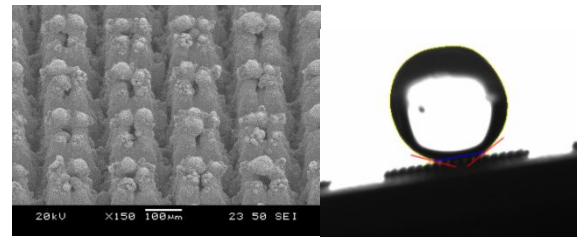


(a)

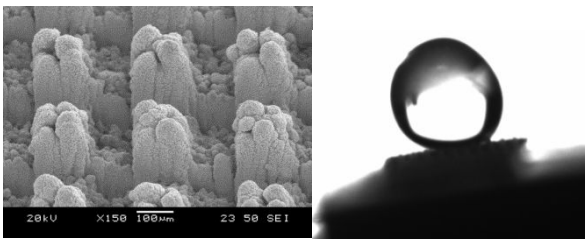


(b)

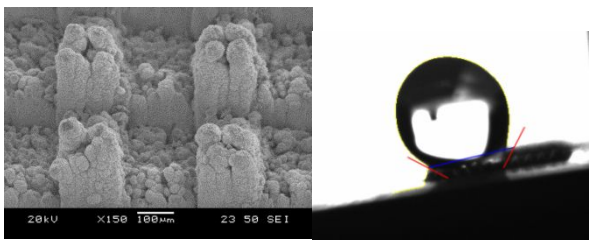


(c)

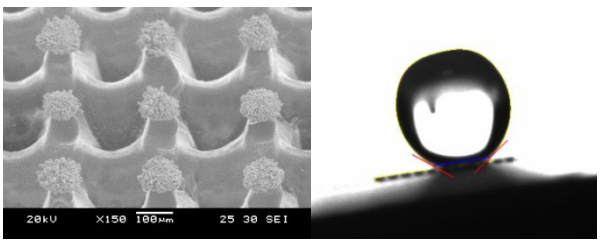


(d)

**Figure 6.2** SEM image of tested structure and captured images of the sliding test: fabricated structure using hierarchical structure in (a) 180 µm, (b) 280 µm and (c) 380 µm spacing, and (d) re-entrant structure

**Table 6.1** Roll off angle and contact angle hysteresis of fabricated structure shown in Figure 6.1.

| Experimental set | Roll off angle(˚) | Contact angle hysteresis(˚) |
|---|---|---|
| (a) | 2 | 2 ~ 5 |
| (b) | 8 | 4 ~ 8 |
| (c) | 15 | 7 ~ 13 |
| (d) | 20 | 10 ~ 20 |

## 6.2 Squeezing test

The droplets (3 μl pendant drop of deionized water) were squeezed with a fabricated surface using hierarchical structure in 180 μm, 280 μm and 380 μm spacing and the fabricated surface using re-entrant structure by gradual increase of current density in electrodeposition. The top surface was a PDMS flat surface with hydrophobic coating.

In the fabricated surface in 280 μm and 380 μm spacing, when the droplet was pressed further, the Wenzel state was forced to be formed on the structure. The fabricated surface in 180 μm spacing (Figure 6.1 (a)) shows that the surface recovered the Cassie-Baxter state and there was a negligible amount of hysteresis when the top surface is lifted. In the case of re-entrant structure, the transition to the Wenzel state and the large hysteresis during the lift-off were observed.

The squeezing test shows that the smaller micro pillar spacing was advantageous in the same results of sliding test. In the case of re-entrant structure, the surface was the most hydrophilic in the experiment set because the ratio of the actual area to the projected area is very large according to the re-entrant structure.

(a)

(b)

(c)

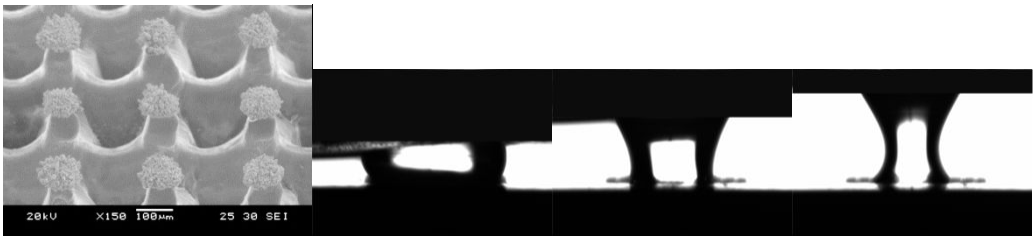


(d)

**Figure 6.3** SEM image of tested structure and captured images of the squeezing test: fabricated structure using hierarchical structure in (a) 180 µm, (b) 280 µm and (c) 380 µm spacing, and (d) re-entrant structure

When the water droplet on the surface of pitch 180 μm was pressed with 600 μm gap, the surface was on wetting state in the contrast with 700 μm gap, shown in Figure 6.4. From the Young-Laplace equation [29], the threshold pressure of non-wet state on the fabricated surface was about 200 Pa. Pressure deduced using the Young-Laplace equation

$$\Delta P = \frac{2\gamma|cos\theta|}{x} \quad , x \ll R$$

$\gamma$ : Surface tension

$\theta$ : Contact angle

$x$ : Gap between the plates

$R$ : Radius of droplet

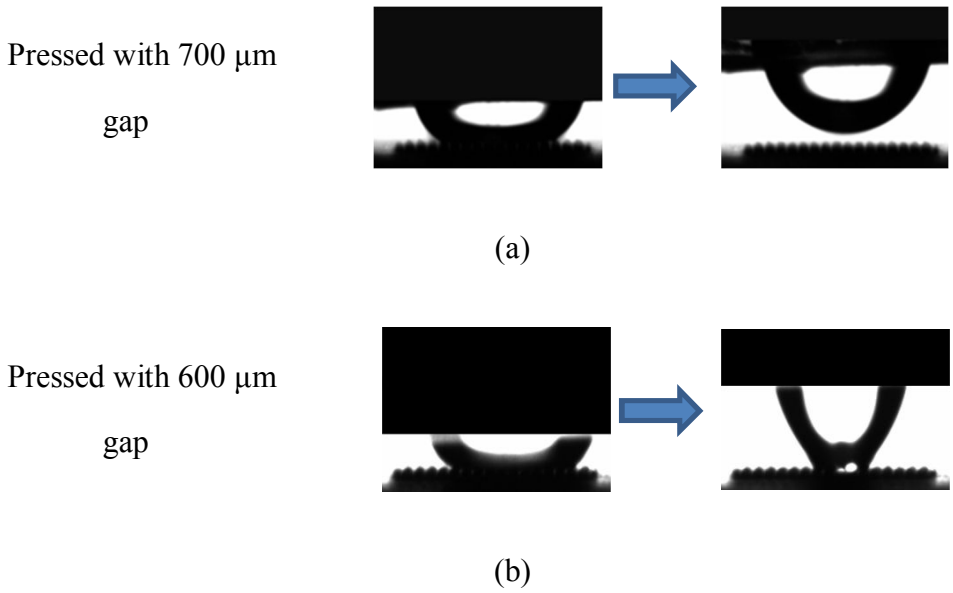


**Figure 6.4** Captured images of the squeezing test: fabricated surfaces with hierarchical structure in 180 μm spacing with (a) 700 μm gap and (b) 600 μm gap

Squeezing test results were analyzed by energy minimization approach [30]. The transition of droplet is process of overcoming energy barrier between Cassie-Baxter and Wenzel states. Transition can be caused by de-pinning of the liquid-air interface from energy minimization and sag transition from geometry of structure. The pressure of the de-pinning transition and the height of the sag transition were calculated by the equations. Theoretical value calculated by the equation from de-pinning transition matched the experimental result of the squeezing test shown in Table 6.2. Increased pitch of the micro pillar lowers the pressure of de-pinning transition. Sag transition didn't be applied to the fabricated structures because they have enough height above 100 μm.

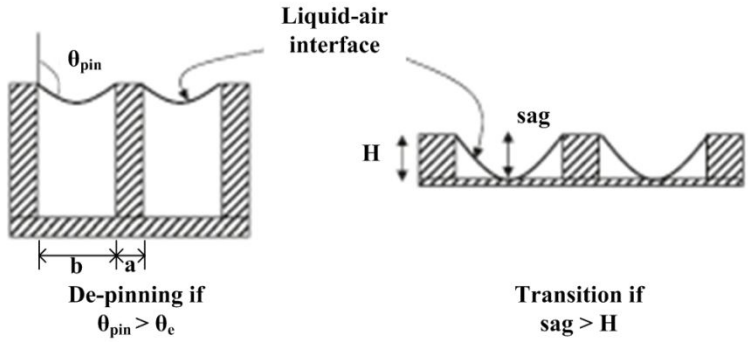


De-pinning transition Sag transition

$$\Delta P > \frac{-4\gamma_{lv}\cos\theta_e}{2b(1+\frac{b}{2a})} \qquad H < R\left(1-\sqrt{1-\frac{b^2}{2R^2}}\right),\ R=\frac{2\gamma_{lv}}{\Delta P}$$

**Figure** 6.5 Side views of the transition from Cassie to Wenzel state due to de-pinning and sag mechanisms in a pillar-type roughness geometry [30]

**Table** 6.2 De-pinning and Sag transition criteria of fabricated structure using hierarchical structure

| Spacing | Pressure(Pa)<br>(De-pinning transition) | Height(㎛)<br>(Sag transition) |
|---|---|---|
| 180 ㎛ | 207±10 | 5.17 |
| 280 ㎛ | 80±5 | 17.8 |
| 380 ㎛ | 43±3 | 36.1 |

# Chapter 7

# Conclusion

The fabrication process of a super-hydrophobic surface, which is a process for re-entrant structure and hierarchical structure, is presented in this paper. Photolithographic methods and polymer type materials have been usually used to fabricate super-hydrophobic surfaces. However, they have some limitations to be applied in practical uses. This paper suggested fabrication process using electrodeposition as a new fabrication method of super-hydrophobic surface on metal. With this method, Super-hydrophobic surfaces were fabricated by physical structures.

In the case of fabrication process for re-entrant structure, super-hydrophobic re-entrant structure array of copper deposition on stainless steel was fabricated. Sequential process of laser ablation, insulation, mechanical polishing and electrodeposition was effective for fabricating re-entrant structure. Experiments for surface morphology relative to the parameter of the laser ablation and electrodeposition were carried out. Under a gradual increase in current density during the electrodeposition, surface morphology roughness was maximized for fabricating a super-hydrophobic surface. Through nickel deposition on stainless steel and copper deposition on copper, material combinations of deposit material and substrate were confirmed.

In the case of fabrication process for hierarchical structure, super-hydrophobic metallic surface with hierarchical structure and copper oxide was fabricated. Under high current density condition in electrodeposition, hierarchical structure with copper oxide was effectively fabricated. In the fabrication process, laser ablation process can be replaced with micro machining process such as

mechanical machining, electrical discharge machining and electrochemical machining with micro structure of above 100 μm depth.

Through the sliding and squeezing tests, the dynamic robustness of hydrophobicity was evaluated. Dynamic wetting property of super-hydrophobic surface fabricated by fabrication process for hierarchical structure was better than that fabricated by sequential process for re-entrant structure due to low surface energy of copper oxide. The results indicate that a fabrication process for hierarchical structure was effective on dynamic wetting property when compared with re-entrant structure. The fabrication process for re-entrant structure is useful on the surfaces that aren't available to form hierarchical structure and copper oxide.

# References

[1] K.S. Liu, X. Yao, L. Jiang, Recent developments in bio-inspired special wettability, Chem. Soc. Rev., 39 (2010) 3240-3255.

[2] M. Morra, E. Occhiello, R. Marola, F. Garbassi, P. Humphrey, D. Johnson, ON THE AGING OF OXYGEN PLASMA-TREATED POLYDIMETHYLSILOXANE SURFACES, J. Colloid Interface Sci., 137 (1990) 11-24.

[3] A. Tuteja, W. Choi, M.L. Ma, J.M. Mabry, S.A. Mazzella, G.C. Rutledge, G.H. McKinley, R.E. Cohen, Designing superoleophobic surfaces, Science, 318 (2007) 1618-1622.

[4] A. Tuteja, W.J. Choi, G.H. McKinley, R.E. Cohen, M.F. Rubner, Design parameters for superhydrophobicity and superoleophobicity, MRS Bull., 33 (2008)

752-758.

[5] L.L. Cao, H.H. Hu, D. Gao, Design and fabrication of micro-textures for inducing a superhydrophobic behavior on hydrophilic materials, Langmuir, 23 (2007) 4310-4314.

[6] M. Karlsson, P. Forsberg, F. Nikolajeff, From Hydrophilic to Superhydrophobic: Fabrication of Micrometer-Sized Nail-Head-Shaped Pillars in Diamond, Langmuir, 26 (2010) 889-893.

[7] B.H. Luo, P.W. Shum, Z.F. Zhou, K.Y. Li, Preparation of hydrophobic surface on steel by patterning using laser ablation process, Surf. Coat. Technol., 204 (2010) 1180-1185.

[8] S. Lyu, D.C. Nguyen, B.S. Yoon, W. Hwang, FABRICATION OF SUPER-HYDROPHILIC/HYDROPHOBIC SURFACE AND DRAG REDUCTION EFFECTS, International conference on composite materials, (2011).

[9] Y. Ohkubo, I. Tsuji, S. Onishi, K. Ogawa, Preparation and characterization of super-hydrophobic and oleophobic surface, J. Mater. Sci., 45 (2010) 4963-4969.

[10] K.S. Liu, L. Jiang, Metallic surfaces with special wettability, Nanoscale, 3

(2011) 825-838.

[11] D. Sarkar, N. Saleema, One-step fabrication process of superhydrophobic green coatings, Surface and Coatings Technology, 204 (2010) 2483-2486.

[12] S. Wang, L. Feng, L. Jiang, One-Step Solution-Immersion Process for the Fabrication of Stable Bionic Superhydrophobic Surfaces, Advanced Materials, 18 (2006) 767-770.

[13] W.G. Bae, K.Y. Song, Y. Rahmawan, C.N. Chu, D. Kim, D.K. Chung, K.Y. Suh, One-Step Process for Superhydrophobic Metallic Surfaces by Wire Electrical Discharge Machining, ACS Appl. Mater. Interfaces, 4 (2012) 3685-3691.

[14] M. Nosonovsky, B. Bhushan, Hierarchical roughness makes superhydrophobic states stable, Microelectron. Eng., 84 (2007) 382-386.

[15] M. Ma, R.M. Hill, Superhydrophobic surfaces, Current Opinion in Colloid & Interface Science, 11 (2006) 193-202.

[16] J.L. Liu, X.Q. Feng, G.F. Wang, S.W. Yu, Mechanisms of superhydrophobicity on hydrophilic substrates, J. Phys.-Condes. Matter, 19 (2007) 12.

[17] C.-K. Hu, J. Harper, Copper interconnections and reliability, Materials Chemistry and Physics, 52 (1998) 5-16.

[18] M. Rahman, Fabrication of EDM electrodes by localized electrochemical deposition, International Journal of Precision Engineering and Manufacturing, 9 (2008) 75-80.

[19] A. Iwamoto, K. Sudoh, T. Yoshinobu, H. Iwasaki, TRANSITION OF GROWTH MODE IN ELECTROCHEMICAL DEPOSITION OF COPPER: ATOMIC FORCE MICROSCOPY ANALYSIS AND SIMULATION, Scanning Microscopy, 12 (1998) 9-15.

[20] T. Bergstresser, H. Merchant, Surface morphology of electrodeposits, Defect Structure, Morphology and Properties of Deposits, (1995) 115-168.

[21] A. Kaldos, H.J. Pieper, E. Wolf, M. Krause, Laser machining in die making - a modern rapid tooling process, J. Mater. Process. Technol., 155 (2004) 1815-1820.

[22] S.W. Lee, H.S. Shin, C.N. Chu, Fabrication of micro-pin array with high aspect ratio on stainless steel using nanosecond laser beam machining, Appl. Surf.

Sci., 264 (2013) 653-663.

[23] D. Quere, Non-sticking drops, Rep. Prog. Phys., 68 (2005) 2495-2532.

[24] M. Voinea, C. Vladuta, C. Bogatu, A. Duta, Surface properties of copper based cermet materials, Materials Science and Engineering: B, 152 (2008) 76-80.

[25] G. Qu, S.S. Vegunta, K. Mai, C.J. Weinman, T. Ghosh, W. Wu, J.C. Flake, Copper Oxide Removal Activity in Nonaqueous Carboxylic Acid Solutions, Journal of The Electrochemical Society, 160 (2013) E49-E53.

[26] L. Gao, T.J. McCarthy, Contact angle hysteresis explained, Langmuir, 22 (2006) 6234-6237.

[27] Y. Kwon, N. Patankar, J. Choi, J. Lee, Design of surface hierarchy for extreme hydrophobicity, Langmuir, 25 (2009) 6129-6136.

[28] K. Kurogi, H. Yan, K. Tsujii, Importance of pinning effect of wetting in super water-repellent surfaces, Colloids and Surfaces A: Physicochemical and Engineering Aspects, 317 (2008) 592-597.

[29] A. Lafuma, D. Quéré, Superhydrophobic states, Nature materials, 2 (2003) 457-460.

[30] N.A. Patankar, Consolidation of hydrophobic transition criteria by using an approximate energy minimization approach, Langmuir, 26 (2010) 8941-8945.

# 국문 초록

본 논문에서는 전해 디포지션을 이용한 금속의 초소수성 표면 제작 방법을 개발하였다. 기존의 초소수성 응용 연구는 자정(self-cleaning), 오염 방지 등을 위한 폴리머 류의 필름 또는 패드 형태로 제한되어 그 응용 가능성에 비해 실제로는 폭넓게 이용되지 않고 있다. 이러한 한계를 극복하고자 초소수성 금속성 표면을 제작하는 공정을 개발하였다. 소수성을 구현하는데 유리하다고 알려진 리엔트런트(re-entrant) 구조의 제작 공정과 계층 구조의 제작 공정을 제안하였다. 리엔트런트 구조는 친수성 재질에도 소수성을 구현할 수 있는 구조로서 이를 형성시키기 위한 제작 방법으로 레이저빔 가공, 절연, 폴리싱, 전해 디포지션의 순차적인 공정을 이용하였다. 미세 구조의 간격은 레이저빔의 조사 경로에 따라 조절이 가능하고, 리엔트런트 구조의 표면 표면 거칠기는 전해 디포지션 공정에서의 전류 조건에 의해서

결정된다. 이를 이용하여 제작한 리엔트런트 구조 어레이가 소수성을 나타내는 것을 확인하였고, 전해 디포지션 공정에서 전류 밀도를 점진적으로 증가시켰을 때, 표면 거칠기가 극대화되어 초소수성을 나타내었다. 계층 구조를 제작하기 위한 공정은 보다 간략한 공정으로서 레이저빔 조사에 의해 형성된 미세 구조에 전해 디포지션을 수행하여 초소수성 표면을 제작하였다. 디포지션 공정 후에 형성된 산화 구리가 표면 에너지를 낮추는 역할을 함으로써 계층 구조에 의한 초소수성이 가능해진다. 100 $\mu$m 이상 깊이의 미세 구조를 갖는 구조에 전해 디포지션을 수행하면 초소수성 표면을 제작할 수 있는 것을 확인하였고, 이러한 미세 구조 형성 공정은 레이저빔 가공 이외의 다른 가공법으로 대체 가능하다. 제작된 표면의 젖음성을 평가하기 위하여 정접촉각, 동접촉각, 압력에 의한 영향을 시험하였다.

**주요어: 초소수성, 젖음성, 금속, 전해 디포지션, 리엔트런트 구조, 계층 구조**

**학 번: 2009-30159**

Ph. D Dissertation Information

Submitted to the School of Mechanical and Aerospace Engineering and the Committee on Graduate Studies of Seoul National University in Partial Fulfillment of the Requirements for the Degree of Doctor of Philosophy

**Title**: Fabrication of a Super-hydrophobic Surface on Metal Using Electrodeposition

**Keywords**: Super-hydrophobicity, Wettability, Metal, Electrodeposition, Laser ablation, Re-entrant structure, Hierarchical structure

**Author**: Min Ho Kwon

**Advisor**: Professor Chong Nam Chu

**Laboratory**: Precision Engineering & Manufacturing Lab., Seoul National University

**Contact**: kwon1351@snu.ac.kr, http://prema.snu.ac.kr

Date: January 27, 2014

© Copyright 2014

By

Min Ho Kwon

All Rights Reserved